Thesis for the Degree of Master of Science

Thermal Analysis and Design of a Cryogenic Cooling System for 10 MW Class High-Temperature Superconducting Generators for Wind Turbine

Le Thanh Dung

Faculty of Applied Energy System

Major of Electrical Engineering

GRADUATE SCHOOL

JEJU NATIONAL UNIVERSITY

AUGUST 2015

Thermal Analysis and Design of a Cryogenic Cooling System for 10 MW Class High-Temperature Superconducting Generators for Wind Turbine

Le Thanh Dung

(Supervised by Professor Ho Min Kim)

A thesis submitted in partial fulfillment of the requirements

for the degree of Master of Science

August 2015

This thesis has been examined and approved

Prof. Gae-Myoung Lee.......이 개명............................

Prof. Ho-Chan Kim...........김 호찬.......................

Prof. Ho Min Kim............김 호민....................

Faculty of Applied Energy System
Major of Electrical Engineering
GRADUATE SCHOOL
JEJU NATIONAL UNIVERSITY

Contents

Acknowledgements

Many persons and organizations have directly or indirectly contributed to my work during the past two years. It is a pleasure to acknowledge the persons and organizations who played an important part in making this thesis possible, without any of which it would have been impossible to complete this thesis.

First, I would like to acknowledge the help of my thesis supervisor, Professor Ho Min Kim, for his support, guidance and encouragement. I would like to extend thanks to the members of High Magnetic Field Energy Lab - Ji Hyung Kim and Sa Il Park, for their useful discussions and suggestions. Special thanks to Ji Hyung Kim for his valuable both technical and personal assistance.

Furthermore, I would like to thank all my friends and colleagues in Electrical, Electronics and Telecommunications Engineering Department, Can Tho University of Technology. Special thanks to Vo Minh Thien and Quach Ngoc Thinh who are always strongly believe me and let me have this great chance. Let me a chance to honorably mention Nguyen Giang Son for his valuable time and difficulties.

Finally, I sincerely thank to my parents, siblings for their help, personal sacrifice and continuous moral support, and to my niece Hong Vy, my nephew Gia Bao whose cheerful ways always make me happy. Furthermore, I would like to express thanks to my love Kim Lieu, for what you have ever done and if there will ever be, you always have the warmest place in my mind.

List of Figures

List of Tables

List of Symbols

I_{op}	Operating current (A)
T	Temperature (K)
ℓ	Length of current lead (mm)
d	Diameter of current lead (mm)
A	Cross section of current lead (m^2)
ρ	Electrical resistivity (Ω.m)
k	Thermal conductivity (W.m^{-1}.K^{-1})
Q_{lead}, Q_{loss}	Current lead loss (W)
A_h	Cross section of HTS tape (m^2)
k_h	Thermal conductivity of HTS tape (W.m^{-1}.K^{-1})
Q_{ff}	Heat flux flow loss (W)
ρ_{ff}	Flux flow resistivity (Ω.m)
$2a$	HTS thickness (mm)
$2w$	HTS width (mm)
$N_v(k)$	Number of vortices per unit length and ampere (m^{-1}A^{-1})
N_{v0}	Number of pinning centers per unit length and ampere (m^{-1}A^{-1})
I_v	Pinning strength (A)
τ	Decay time
L_{cu}	Inductance of copper stabilizer (μH)
ℓ_{cu}	Length of copper stabilizer (mm)
A_{cu}	Cross sectional area of copper stabilizer (mm)
Q_t	Torque tube conduction loss (W)
δ_t	The torque tube length (mm)
A_t	The torque tube equivalent cross-sectional area (mm)
σ_t	The torque tube torsion angle (°)
α	Coefficient of thermal expansion (1/K)
L	The torque tube initial length (mm)
Q_r	Radiation loss (W)

ε	Thermal emissivity of the material
σ	Stefan-Boltzmann constant (5.67×10^{-8} W.m^{-2}.K^{-4})
S_r	Radiation area (m^2)
Q_g	Conduction heat loss of residual gas (W)
η_g	Accommodation coefficient
P_g	The pressure of the gas in the Dewar (Torr)
S_g	Cross-section facing the radiation shields (m^2)
Q_j	Joule heating loss (W)
R_j	Total joint resistance (Ω)
N_j	Total number of mechanical lap joint of HTS tapes
H_m	Magnetic field (T)
μ_0	The permeability of free space ($4\pi \times 10^{-7}$ H/m)
λ	Fraction of superconductor in the composite cross-section
ρ_m	Matrix resistivity (Ω.m)
τ_m	Time constant of the system
E_c	Electric field criterion (V)
l_{mx}	Conductor length (m)
L_m	The magnet of inductance (H)
I_c	Critical current (A)
Q_{conv}	Natural convection cooling of finned surface (W)
h_c	Heat transfer coefficient (W.m^{-1}.K^{-2})
A_c	Heat transfer surface area (m^2)
S_{opt}	Optimum spacing (mm)
ℓ_{fin}	Fin length (mm)
Q_{total}	Total loss of HTSSG rotor (W)
Δt	Duration (h)
ΔH	Total enthalpy change of solid cryogen (J.cm^{-3})
C_p	The specific heat of the solid cryogen (J.cm^{-3}.K^{-1})
V_{sc}	Total volume of the solid cryogen vessel (l)

Summary

A cooling system is an essential part of high-temperature superconducting (HTS) rotating machine manufacturing. Moreover, thermal behavior is a crucial parameter of the cooling system that shows unique characteristics of superconductivity below a specific temperature to maintain a superconducting state. Therefore, many experiments have been performed to investigate new reliable cryogenic cooling systems for a large-scale HTS rotating machine. The motivation for this thesis is the development of a cryogenic cooling system using thermal trigger switches; it effectively minimizes non-operational downtime of the HTS machine in cases of power supply or cryocooler failure. Hence, a HTS rotating machine will not be affected by this failure because it is going to be continuously supported by "thermal battery" using solid nitrogen within a period of time.

This thesis focuses on two main targets. First, the thermal design of the cooling system for the 10 MW-class HTS synchronous generator (HTSSG) is enhanced to diminish thermal absorption from room temperature whenever the cryocooler fails. This step focuses on the most major losses of (1) generator rotor losses including conduction loss of current leads, conduction loss of torque tubes, radiation loss, superconducting losses (taking account on mechanical lap joint Joule heating loss and intrinsic n-value loss), and (2) conduction loss of system supporting rods and natural convection occurring in heat exchanger, as well. To get maximum elimination these losses, the numerical method was applied to optimize the design of a current lead and a torque tube, respectively.

Finally, the possibility of constructing HTS field coil can be maintained a constant low temperature without an external power source or an external supply of cryogen is demonstrated. Hence, the performance of the cooling system is observed for various cryogens to investigate the feasibility of using solid cryogen as a "thermal battery". It will optimize total volume of solid cryogens to remain in the HTS field coils, which are kept in a cryostat, and are kept below a certain temperature as long as desired.

Chapter 1. Introduction

1.1 Background
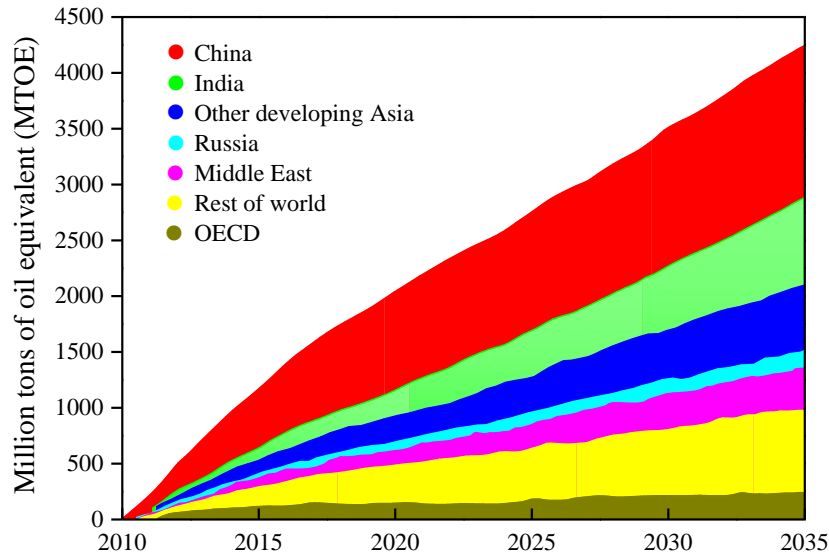
Fig. 1. Growth in primary energy demand in the New Policies Scenario (IEA 2014)

Nowadays, the need of energy has been increasing day by day with the population growth and the advancements of technology. In Fig. 1, it is estimated that the global energy demand will roughly increase four times in 2035 with over 4000 million tons of oil-equivalent (MTOE) compared to 2015 (1000 MTOE) [1]. Therefore, energy security is no longer only about oil, and industrialized nations are no longer the only major consumers of energy. Climate change driven by greenhouse gas emissions – 70% of which derive from energy production or use – is a growing threat.

To overcome this challenge, the world will use renewable energy instead of using fossil fuels in order to meet the demands of the world's energy. Fortunately, wind energy currently is seen as a positive alternative to fossil fuels and also a way to assist the expansion of local economies in future. The wind energy production of recent years has risen in a high and linear evolution of the growth of electrical energy. Also, a high growth of wind turbines capacity is expected to be installed in following decade. Fig. 2 shows that the total installed wind capacity constantly increases annually [2]. In the end of 2014, total installed wind capacity is 360 MW, it increased 50 % compared to 2011.
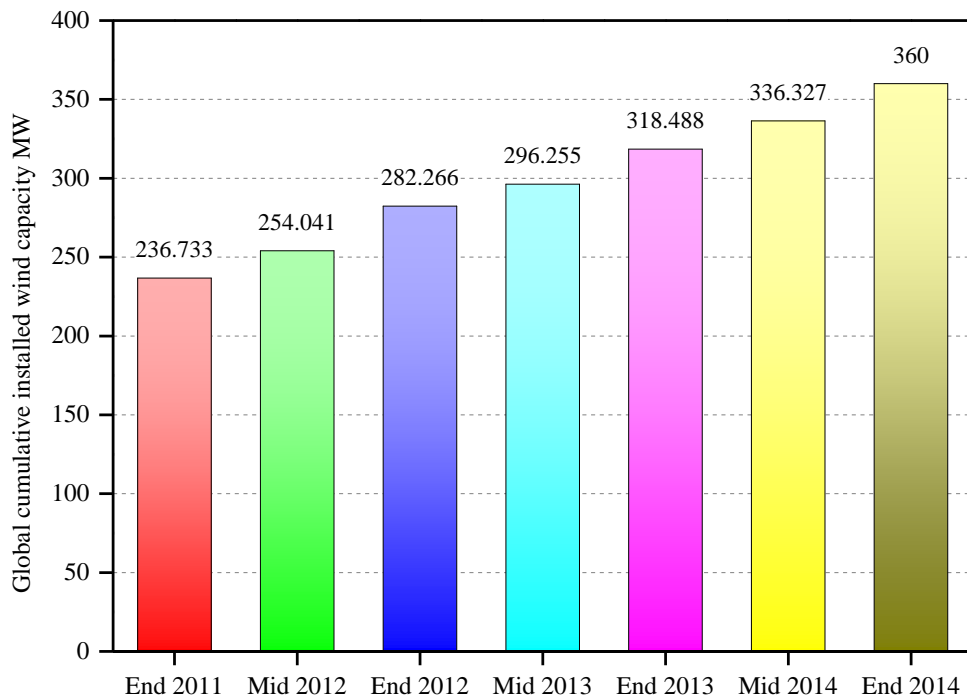
Fig. 2. Wind power total world installed capacity 2011-2014 in MW (WWEA 2015)

In addition, there is also a trend showing an increase in the average wind turbine unit rating every year with the prospects of the higher than 8 MW wind turbine project concept designs and installations for the coming decade [3]. However, for wind turbine electric ratings higher than 8 MW, its geometric dimensions and consequently the total weight of the generators increase exponentially. For this main reason, it is required to search for alternative technologies for offshore wind turbines with powers more than 8 MW to achieve the electrical power with a lower electrical generator volume and a low total weight with reasonable costs.

Fortunately, the result of the high current density in HTS tape obtained in HTSSGs bring a great deal of advantages. The conventional copper coil in a conventional machine typically operate with a maximum current density 5 A/mm^2 while the current density in the HTS wire can operate at 200 A/mm^2 [4]. As a consequence a higher induction could be obtained by using HTS coils; for this reason HTSSGs hold the potential of providing high torques in a smaller size and with a smaller weight than conventional technologies [5]. Because the lower dimensions required a lower weight compared with conventional machines of the same electric rating and nominal speed is

Table 1. HTS direct drive wind turbine technology conceptual design

Company/Project	Model	Power (MW)	Status/year
Azimut Project		15	Concept/2020
GE		15	Concept/-
AMSC	Sea Titan	10	Prototype/2011
TECNALIA	SUPRAPOWER	10	Concept/2016
SUPERPOWER	REACT	10	Concept/2013

needed, it is proving to be attractive for wind energy. Moreover, a HTSSG has the best indicators including different technical, environmental, and economical aspects, for example, maintenance-free, smaller size, simpler structure and higher reliability considered to a evaluate various types of wind turbine generators – such as squirrel-cage induction generator (SCIG), doubly-fed induction generator (DFIG), multi-phase induction generator (MPIG), synchronous generator (SG), electrically excited synchronous generator (EESG), permanent magnet synchronous generator (PMSG) - for specific applications [6]. Therefore, it is increasing number of research and development projects to focus on HTSSG nowadays. As indicated in Table 1, the highest number of currently wind turbine projects in developments for more than 10 MW, and all of them have a direct drive transmission system.

However, there are two major challenges which must be addressed before a large scale utilization can be obtained. The first is the price of the superconducting wires. Because of a huge progress has been made worldwide in increasing the length, performances, price trends for coated conductors in the last 10 years and the achieved improvements in performance of coated conductors produced at an industrial basis, it is assumed that superconducting wire can be manufactured at a cost of less than $5/kAm in the future. It is estimated that this should occur in the time frame 2025-2030 and that by 2020 the price should already come down to $20-40/kAm [7]. While SuNAM gives an achievable estimation to get the price reduce to $100/kAm in next two years (2017), and less than $50/kAm in 5 years later [8].

Table 2. Suggested cooling method for HTS machines

Power rating	Rotate speed	Suggested method
Small	High	Thermo-syphon
Large	High	Open evaporative cooling
Small, large	Low	Pipe evaporative cooling

The second challenge is to demonstrate the reliability of the technology seen from a system perspective including the cooling technology. Among particular sub-system: HTS windings, electromagnetic shield, heat insulation, the cooling system is one of the important components of HTS machines whose function is to take heat away rapidly and maintain the superconducting property. Therefore, the robust and reliable cooling system is required for HTS machines to operate for a long time. Relative to the development and improvement of HTS machines, investigations on the cooling system are also enhanced. The recommended cooling methods for HTS machines rotor are based on phase change heat transfer as listed in Table 2 [9]. For motors with low rotate speed, pipe evaporative cooling is strongly recommended as an innovative cooling to avoid low centrifugal acceleration. It has also been successfully applied to 1.5 MWA and 5 MW HTS motors prototypes in 2002 in USA [10]-[11].

Furthermore, in cases of the magnet must be run in stand-alone mode, in which access to a power supply to simultaneously run the cryo-cooler is not available. A stand-alone solid nitrogen cooled permanent high-temperature superconducting magnet system has been successfully proposed and presented [12]. Because of the achievement of this portable design, it significantly offers three improvements for energy applications applied a HTS magnet (1) enhanced thermal stability of HTS magnet; (2) simpler system dynamics; and (3) improved portability feasible with a cryo-cooler that is removed while the system is in operation. Therefore, this thesis will proposed a reliable cooling system for a 10 MW class HTSSG for wind power generation based on those recent achievements above. A detailed objective of thesis will be outlined in next section.

1.2 Thesis objectives
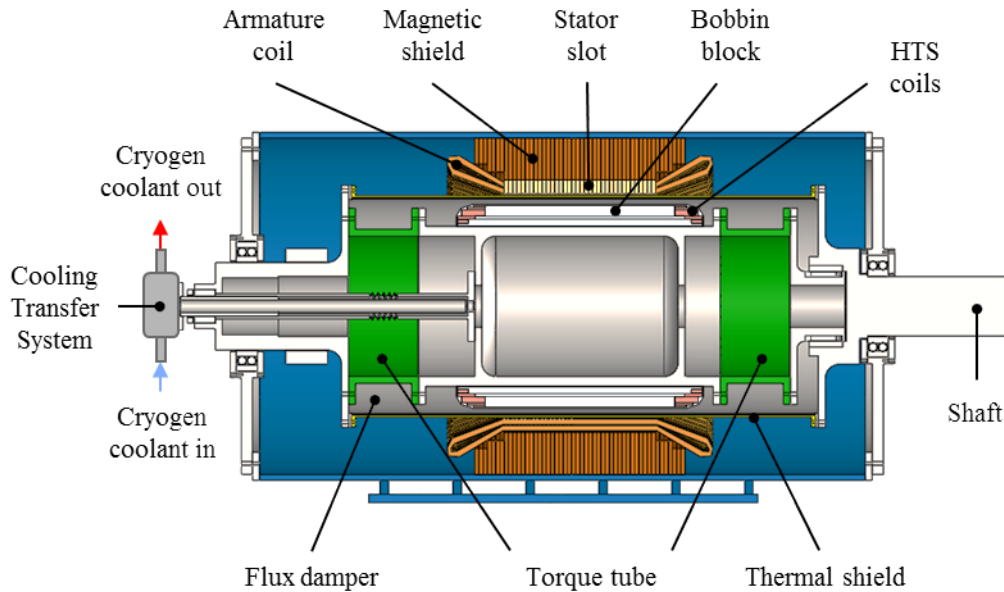
Fig. 3. Basic schematic view of a HTS rotating machine conceptual design

In consideration of advantages and developments in the 10 MW HTSSGs for wind power generation, we have proposed a recent study optimizing design specifications for a 10 MW class HTSSG wind power in terms of electromagnetic and electrical design [13];[14], and the optimal design specifications are listed in Table 3 and Table 4.

We will continue this thesis whose first objective is to optimize the thermal losses. The optimization philosophy is based on producing a thermal design which will require the least amount of refrigerator power while satisfying all other rotor design requirements, as basically shown in Fig. 3. It provides a comprehensive view of the behavior and performance of conduction-cooled current leads, and torque tubes for superconducting magnets. Based on this understanding, specific recommendations are made for the design of a current lead and a torque tube for rotating winding.

A final objective which is carefully providing a clear overall picture of the state of the art in cryogenic systems design for superconducting rotors. This section illustrates a design example of stand-alone cooling system. The stand-alone cooling system reproduces the design problem which will be encountered in simultaneously cooling down HTSSG rotor field coil during period of time in cases of the cryocooler failures.

Table 3. The main specifications of a 10 MW HTSSG for wind turbine

Design parameter specifications	
Rated output (MW)	10.02
Frequency (Hz)	2
Rotating speed (rpm)	10
Terminal voltage (kV)	6008
Rated torque (MN.m)	9.55
Efficiency (%)	96.326
Synchronous reactance (p.u)	0.1
Power factor	1
Weight (ton)	135
Volume (m^3)	40.74

Table 4. The optimized design parameters for HTS rotor field coil and stator

HTS field coil		Armature coil and stator	
Wire	2G HTS	Conductor	Flat type copper
Field coil type	Racetrack	Winding type	Double layer & full pitch
Winding type	Double pancake	Stator slot	144
Field coil current (A)	232	Armature coil current (A)	962
Total winding number	229170	Stator coil number (per phase)	384
HTS wire length (km)	1077	Copper wire length (km)	6482
Current density (A/mm^2)	137.9	Current density (A/mm2)	3
Operating temperature (K)	35	Insulating class	F
Maximum magnetic field density (T)	11.38	Maximum magnetic field density (T)	2.5

Chapter 2. Thermal Loss Analysis

2.1 Current lead loss

Certainly, there are several types of current leads are being used for the superconducting magnet system. It can be generally classified as: metal lead, partially HTS lead (a combination between metal section and HTS section), full HTS lead - then combined with conduction cooled or vapor cooled method, respectively, as shown in Table 5. To minimize heat loss through current lead and increasing efficiency cool down of the lead, conduction cooled lead is selected for this design.

A basic schematic design of current leads for a large scale HTS rotating machine is illustrated in Fig. 4. It's easily seen that, there are two ranges of temperature – between 300 and 80 K, and others within 80 and 30 K. The second term of temperature range is surely suitable for HTS materials under their operation temperature, so we also concern the partially HTS lead among the conventional metal leads design.

Consequently, two critical causes for heat loss along the leads are conduction heat loss and dissipation of Joule heating loss. The major difficulties in carrying out calculations on leads are linked with the fact that the electrical resistivity and heat conductivity of the material from the leads. They rely on the temperature distribution along the lead's length. To figure out this issue, numerical solution is derived instead of complexly analytical solution.

We will conceptually design and analyze steady-state thermal characteristic for two types of lead 1) conventional metal lead with two different materials: brass and copper 2) partially HTS leads with the HTS section (YBCO tape is used) attached to metal support structure.

Table 5. Different types of current leads

Cooling method	Conduction cooled		Vapor cooled lead
Material	Metal (Brass, Copper)	Metal + HTS current lead (hybrid type)	HTS current lead
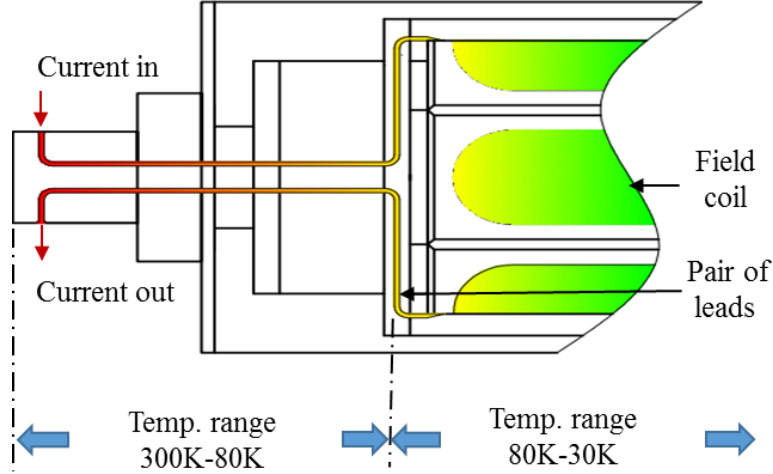
Fig. 4. Basic schematic view of conceptual design for one pair of current leads

Table 6. Parameters of current lead at operating current $I_{op} = 232$ A

Part I Temp. range 300K-80K	T_1	300 (K)	High temperature end
	T_2	80 (K)	Cold temperature end
	ℓ_1	1534 (mm)	Length of lead
Part II Temp. range 80K-30K	T_3	80 (K)	High temperature end
	T_4	30 (K)	Cold temperature end
	ℓ_2	1667 (mm)	Length of lead

2.1.1 Conventional metal lead

For a conduction cooled metal lead operating between room-temperature and cold end temperature, the steady state lead power differential equation over a unit lead length is given by [15]:

$$A\tilde{k}T\frac{d^2T}{dz^2} + \frac{\tilde{\rho}TI_0^2}{A} = 0 \tag{1}$$

where A is cross sectional area of the lead; k and ρ are thermal conductivity and electrical resistivity of the lead material, respectively, listed on Table 6. Then, we obtain an optimized lead that minimizes loss Q for given current I with the optimal length-cross section ratio ℓ/A which depends on working temperature and material properties is expressed by Eq. 2, where represents length along of axis direction and the boundary

Fig. 5. Schematic of variable diameter metal conventional current lead

condition $T(z = 0) = T_0$, $T(z = \ell) = T_\ell$, and then total heat loss Q will have a minimum value as shown in Eq. 3.

$$\left(\frac{Il}{A}\right) = \sqrt{\frac{2\tilde{k}\left(T_l - T_0\right)}{\tilde{\rho}}} \tag{2}$$

$$Q = I\sqrt{2\tilde{k}\tilde{\rho}\left(T_l - T_0\right)} \tag{3}$$

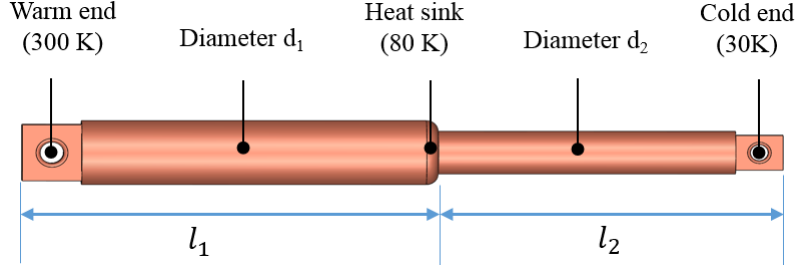However, for Eq. 1, it becomes more difficult, if A is not fixed and relies on z. It's hard to solve the optimal A distribution directly from analytical solution because all parameters in the equation seem to be non-linear. At that time, to clarify this issue, numerical solution is selected. With numerical solution method, different T distribution results in different A distribution. Then heat loss at the cold end of metal lead could be calculated based on the Eq. 4 below accordance with the T distribution.

$$Q_{loss} = \left(k\left(T^{'}\right)A^{'}\frac{dT}{dz} + \rho\left(T^{'}\right)I^2\frac{dTdz}{A^{'}}\right)\Bigg|_{z=l} \tag{4}$$

where T', A' are temperature and cross sectional at $z = \ell$, respectively. Q_{loss} is the total heat loss at cold end for each part of the lead. It simultaneously changes with variation diameter d of the lead, and it is the final target we should optimize, as well. As consequence, metal lead is separated into two parts with different diameter. Its structure is shown in Fig. 5, d_1 and d_2, respectively, are diameter of two parts. With the variation of d_1 and d_2, Q_{loss} definitely has different values. Fig. 6 and Fig. 7 show the dependence of variable diameter current lead for the two different materials - copper and brass, respectively.

Table 7. Mechanical and electrical properties of current lead materials

Material	Properties	Temperature range	
		30 – 80 K	80 – 300 K
Copper	Thermal conductivity $k*$ (W/m.K)	781	460
	Electrical resistivity $\rho*$ (Ω.m)	2×10^{-9}	17.5×10^{-9}
Brass	Thermal conductivity $k*$ (W/m.K)	24	65
	Electrical resistivity $\rho*$ (Ω.m)	47×10^{-9}	70×10^{-9}

$k*$ and $\rho*$ are average value in each range of temperature

Table 8. The optimized parameters of one pair of lead

Material	Parameters	Value
Copper	Diameter part I – d_1 (mm)	12
	Diameter part II – d_2 (mm)	8
	Total weight (kg)	4.6
	Total loss (W)	34.34
Brass	Diameter part I – d_1 (mm)	30
	Diameter part II – d_2 (mm)	51
	Total weight (kg)	78
	Total loss (W)	34.40

On that occasion, the optimal total loss for one pair of lead $Q_{lead} = 2(Q_{loss1} + Q_{loss2})$ is 34.34 W for copper, 34.40 W for brass. The total loss between two types of lead are insignificantly difference just 0.17%. Nonetheless, when we consider the weight of lead, copper is strongly recommended, because cross-sectional area of copper lead (average diameter 10 mm) is much smaller than the brass one (average diameter is 40 mm) while mass density of these materials look like equal, 8960 kg/m^3 and 8530 kg/m^3. As a result, the total weight of copper lead and brass lead is 4.6 kg, and 78 kg, respectively. Table 8 illustrates detail summary optimized specifications of two kinds of lead.
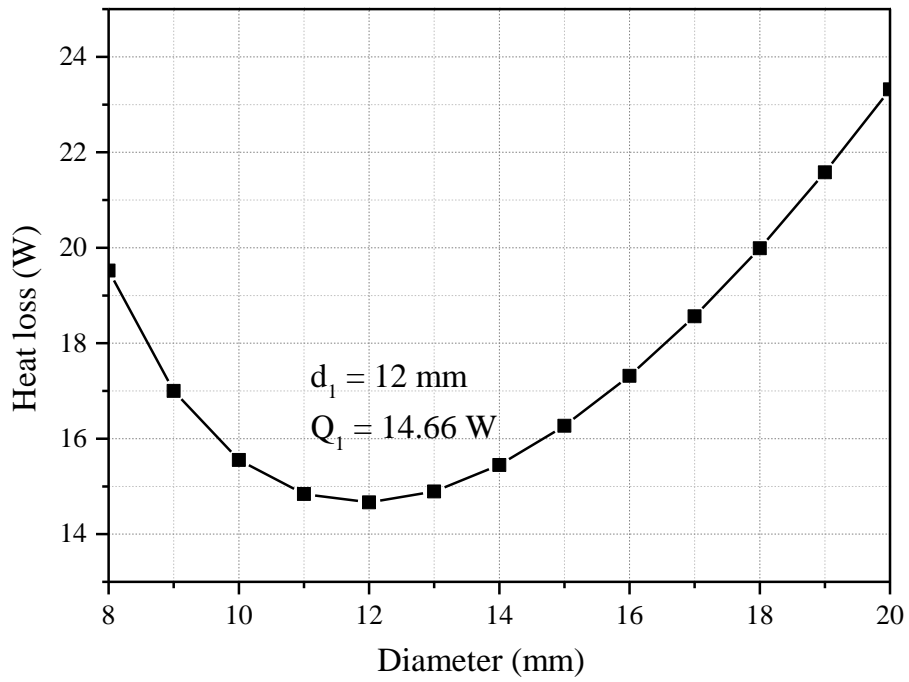
(a)
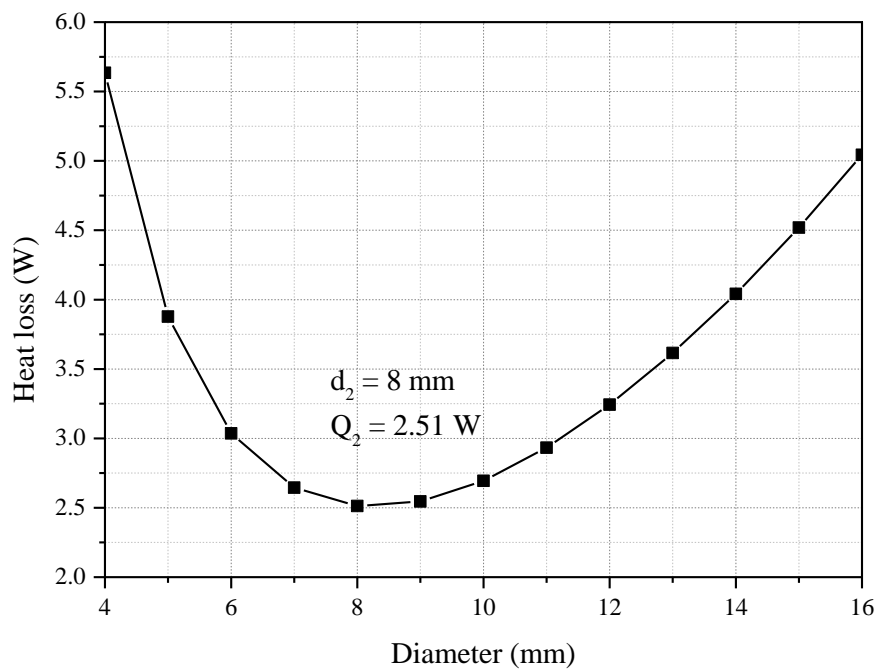
(b)

Fig. 6. The relative between heat loss and diameter of copper lead: (a) part I temperature range from 80 and 300 K, (b) part II temperature range from 30 and 80 K

Fig. 7. The relative between heat loss and diameter of brass lead: (a) part I temperature range from 80 and 300 K, (b) part II temperature range from 30 and 80 K

2.1.2 Partially HTS lead

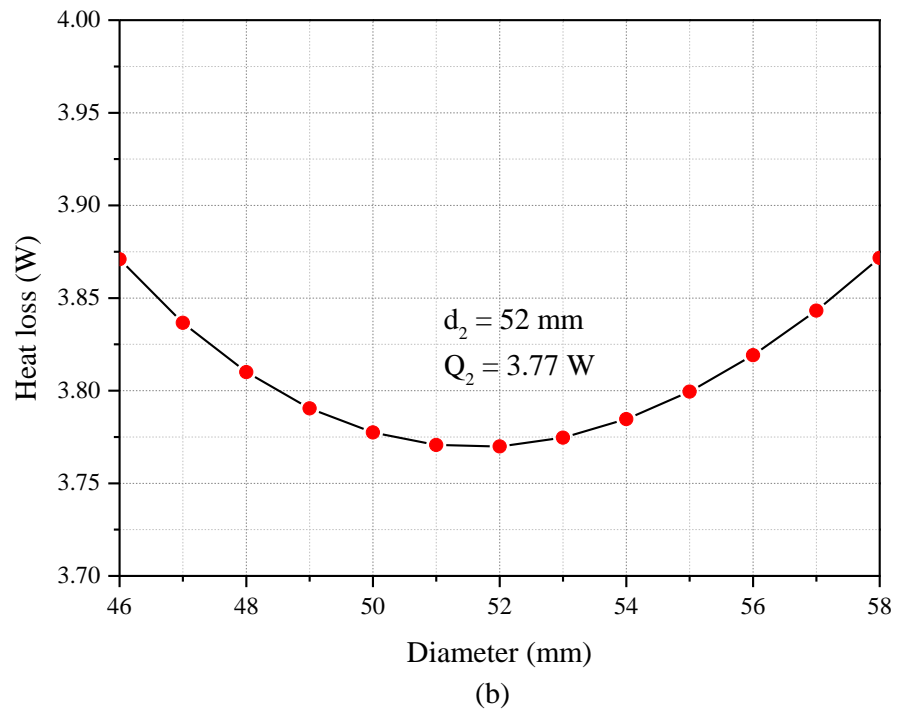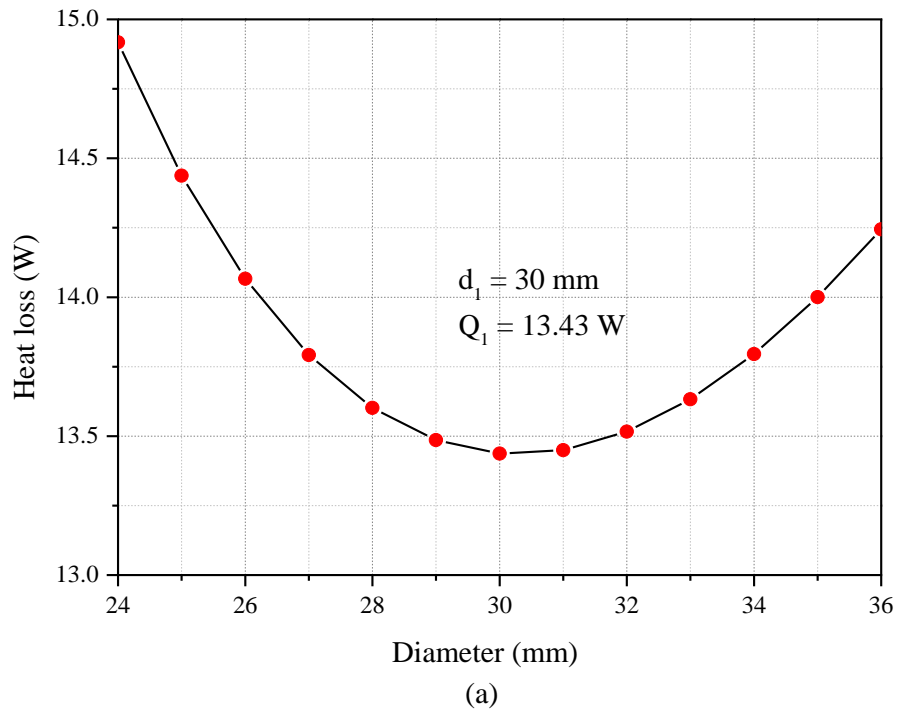To minimize most heat loss of current lead for HTS rotating machine, the choice of conductor properties and lead geometry - such as length, cross section, and cooling surface area - are one of the various significant factors must be selected. Therefore, an optimal lead for large scale of HTS rotating machine has presented before. Not let up with these trends, this section continues to optimize the heat loss of a current lead by proposing a new design of HTS part. Then, the transient thermal characteristics of the lead will be also performed. The loss characteristics will be conducted varying to different current ramp rate at 2.5 A/s, 5 A/s, 10 A/s, respectively. Moreover, a sudden discharge is also mentioned in the simulation, in a certain assumption, the fault condition is occurred, and the flux flow losses exposed by DC current is finally calculated by numerical method [16].

Fig. 8 illustrates the new conceptual design of a HTS partially current lead. It is composed by two side-covers, upper and lower support, which are connected by connection bolts. Then, HTS tapes are occupied inside between the two supports. Because OFHC has a higher thermal conductivity than aluminum, brass, G10, it absolutely leads to higher conduction loss. However, the OFHC considerably enhances the thermal stability of the conduction-cooled HTS coil because of its superior thermal diffusivity. Therefore, OFHC is used for winding the HTS tapes in the partially HTS leads.
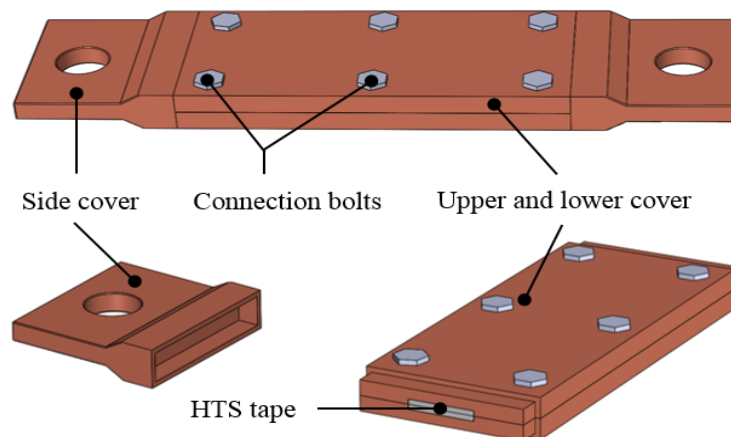

Fig. 8. New conceptual design of a HTS current lead

Table 9. Specifications of the YBCO CC tapes (SCS12050)

Characteristics	SCS12050
Substrate layer	Hastelloy
Stabilizer	Copper
Total stabilizer thickness (mm)	0.1
Total thickness (mm)	0.16
Tape width (mm)	12
Ic at 77 K, self field, 1μV/cm (A)	240
Number of tapes	2
Length of lead (mm)	1667
Total cross section of OFHC copper support (mm^2)	188
Total conduction heal loss (W)	4.67

Table 9 lists the detailed specifications of surround copper stabilizer YBCO coated conductor (CC) used in this study (*SuperPower Inc.*). It is 12-mm wide and 0.16-mm thick. Our system operating current is 232 A, then we simply use two turns of YBCO tape, it means an average current of each tape is 116 A (at the highest temperature 80 K). This value reaches around two times less than the minimum critical current value of the YBCO CC which is over 240 A (at 77 K, self-field condition). Then the average current value of two turns YBCO tape is sufficient to design the current lead. At this time, the total conduction of partially HTS lead is estimated approximately 4.67 W.

Under the condition DC mode, the heat conduction equation for the conduction-cooled HTS current lead is expressed by Eq. 5:

$$\frac{d}{dt}\left[k_h(T)A_h \frac{dT}{dx} \right] + Q_{ff} = 0 \tag{5}$$

where A_h and k_h are cross-section and thermal conductivity of the HTS section, respectively. Q_{ff} is flux flow loss in terms of HTS tape exposed by DC current and magnetic field, and it has been carefully conducted. Flux flow is a state of constant flux

movement, where the pinning force is either non-existent or too small to counteract the Lorentz force. As is the case with flux creep, flux flow is more important in HTS, especially if the operating temperature is close to the critical temperature T_c. The higher the thermal energy of the systems, meaning the closer the temperature is to superconductor's critical temperature, the weaker the pinning forces will be. This is why even HTS perform better at lower temperature.

$$Q_{ff} = \rho_{ff} \frac{I_v^2}{4aw} \exp\left(\frac{N_v(k)}{N_{v0}}\right)\left(\frac{I_{op}}{I_v}\right)^2 \cosh\left(\frac{I_{op}}{I_v}\right) \tag{6}$$

The quantity ρ_{ff} (1.15x10^{-24} Ω.m) plays the role of flux flow resistivity. While $2a$ and $2w$ are HTS thickness and width, respectively. $N_v(k)$ (1.34x108 m^{-1}A^{-1}) is number of vortices per unit length and ampere. N_{v0} (76.8x106 m^{-1}A^{-1}) is number of pinning centers per unit length and ampere. I_v (4.84 A) is pinning strength, and I_{op} is operating DC current which depends on duration and various current ramp rate. Fig. 9 shows the maximum flux flow loss is 0.15 W when the current reaches the peak at 116 A at a 46, 24, 12 second, respectively, in considerations of different ramp rate at 2.5 A/s, 5 A/s and 10 A/s.
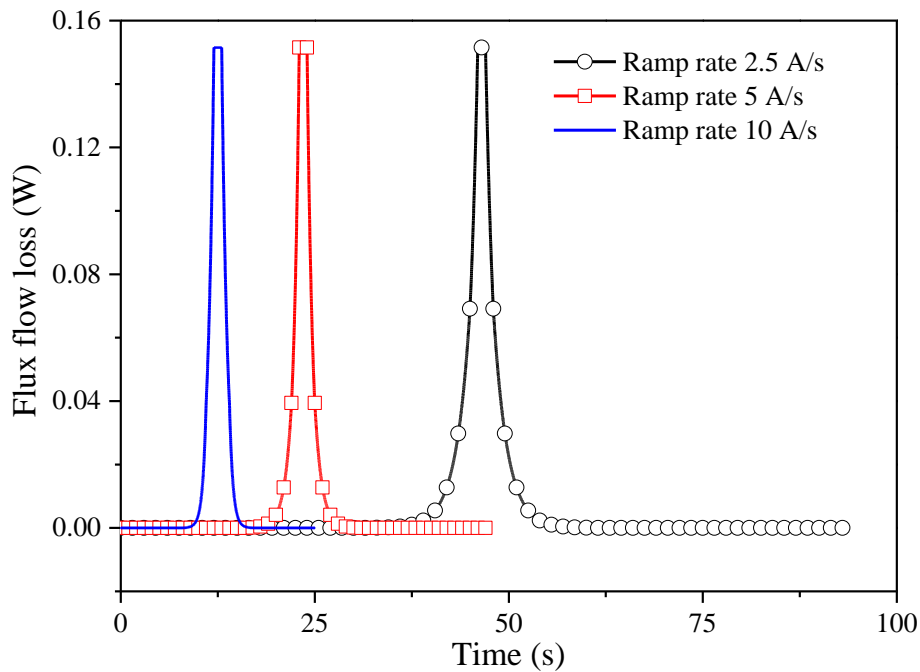
Fig. 9. Flux flow losses varying to current ramp rates

(a)

(b)

Fig. 10. Characteristic of ramp rate at 2.5 A/s (a) eddy current loss, (b) eddy current density of upper and lower copper support

(a)

(b)

Fig. 11. Characteristic of ramp rate at 5 A/s (a) eddy current loss, (b) eddy current density of upper and lower copper support
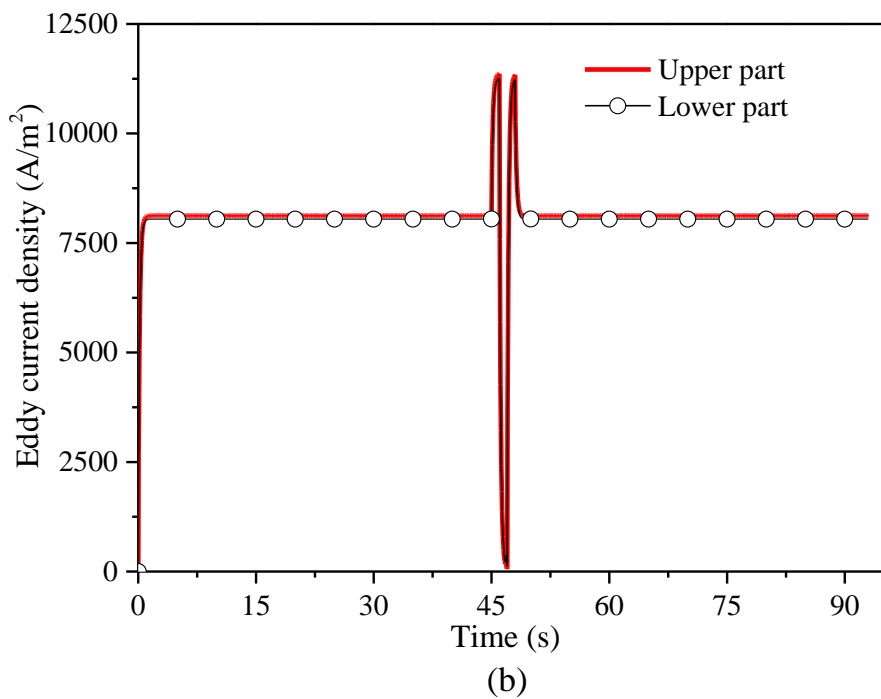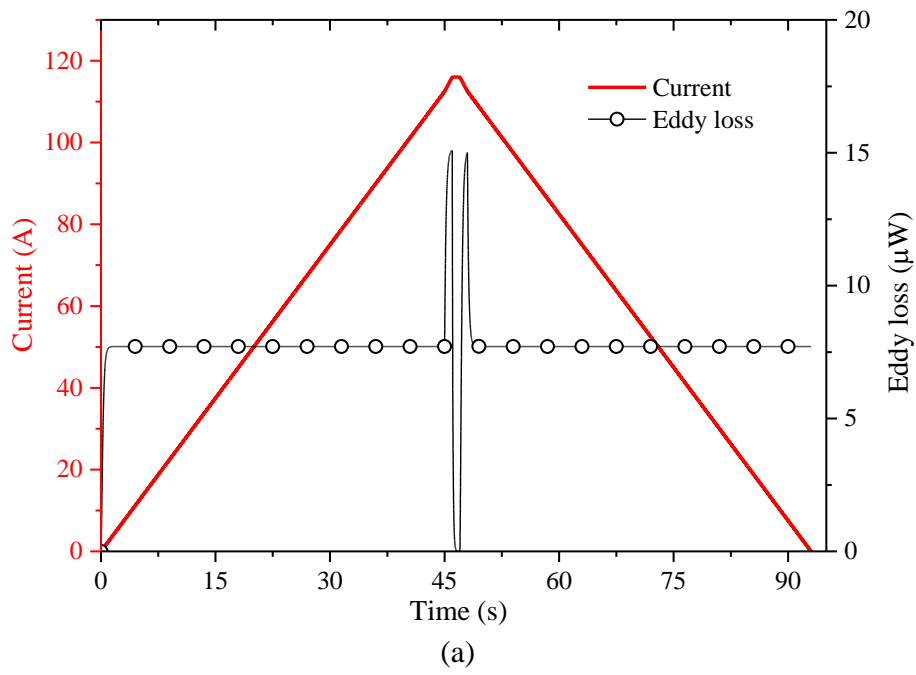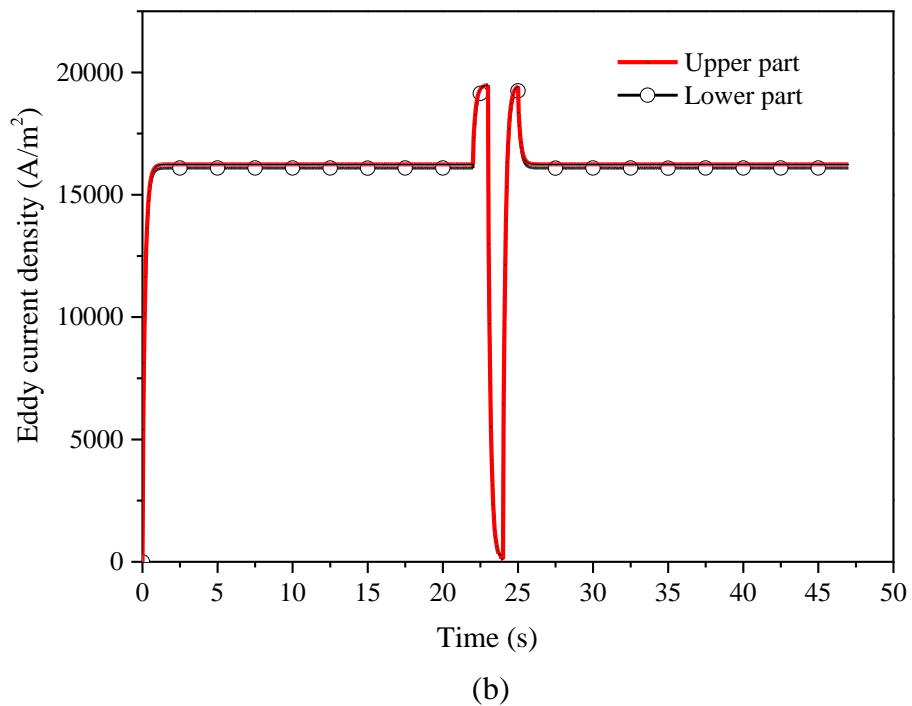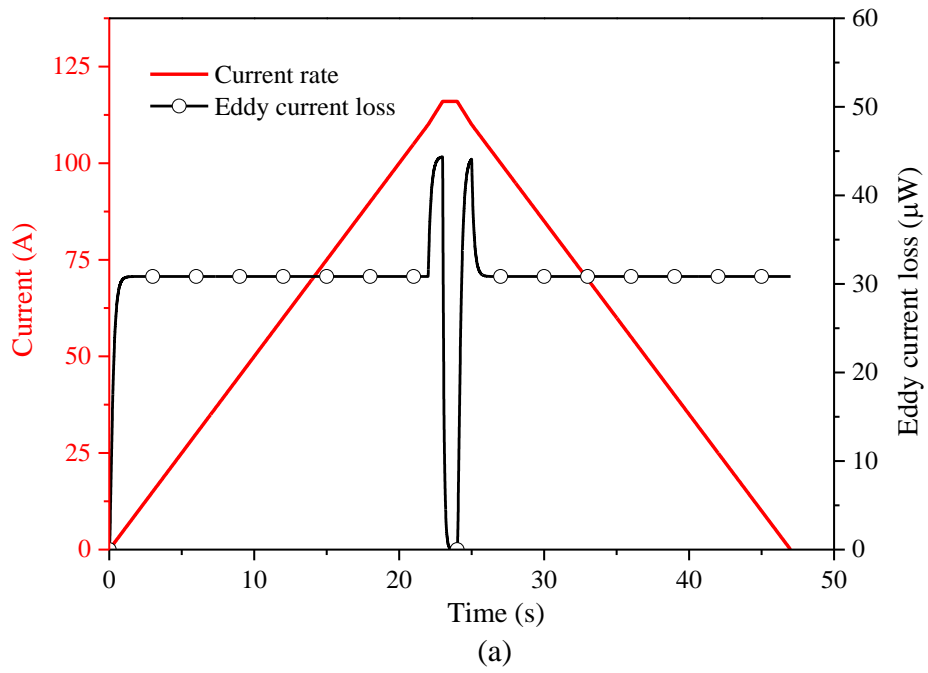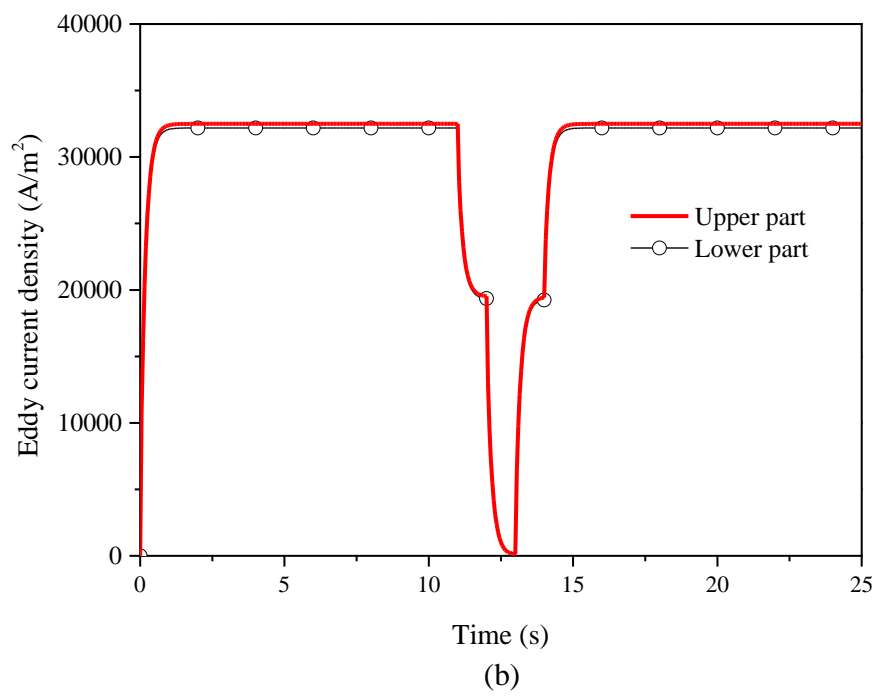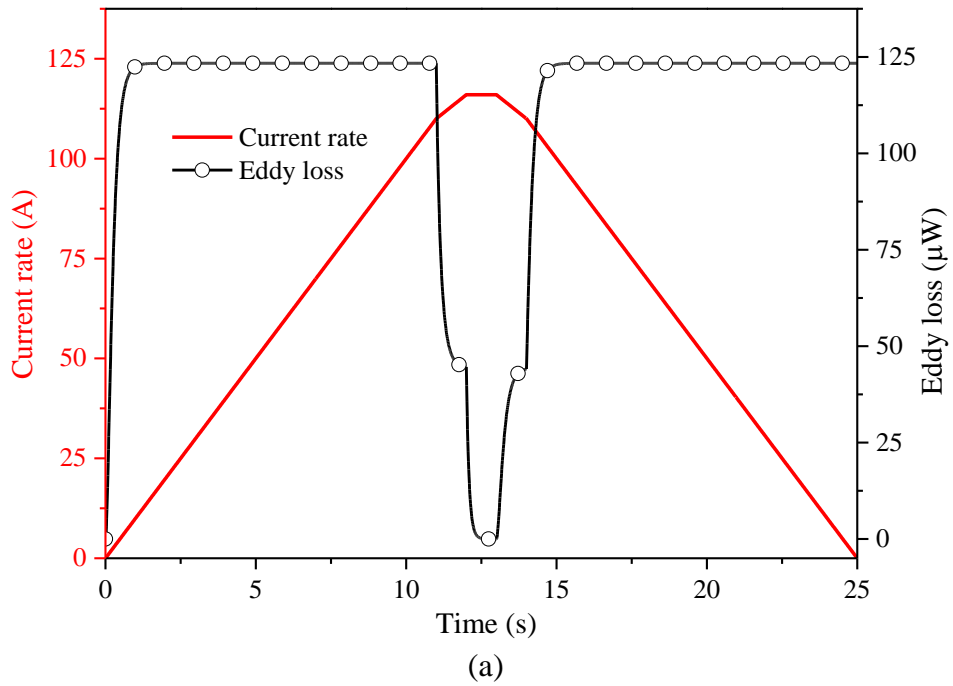
Fig. 12. Characteristic of ramp rate at 10 A/s (a) eddy current loss, (b) eddy current density of upper and lower copper support

Fig. 10, Fig. 11, and Fig. 12 are in succession of illustrating the average eddy current loss and eddy current density of copper support varying to different current ramp rate. It is easily seen that the losses is proportional to current ramp. The faster the ramp rate is, the larger the eddy current loss is deserved. In case of 10 A/s rate, the maximum eddy current is nearly 125 µW, and it decreases to 45 µW, 15 µW for 5 A/s and 2.5 A/s, respectively. Moreover, within ramp rate 2.5 A/s and 5 A/s, respectively, it is seen that the eddy current loss suddenly increases at the last second before the current reaches the peak at 116 A because the current ramp change at the last second. It changed from 2.5 A/s to 3.5 A/s at 45 second and 5 A/s to 6 A/s at 22 second. In contrast, eddy current loss abruptly decreases at 11 second because ramp rate goes down from 10 A/s to 6 A/s in cases of ramp rate 10 A/s.

$$I(t) = I_{peak} e^{-\frac{t}{\tau}} \tag{7}$$

In considerations of fault condition, the equivalent circuit model of a HTS coil is conveniently illustrated in Fig. 13. We assume that the supply current increased to each current level and remained at the level I_{peak} 116 A during the steady state operation, then decreased to 0 A. In this case, the current will flow in the two copper stabilizer instead of HTS layer, where L_1, L_2, and R_1, R_2 are inductance and resistance of the two copper stabilizers, respectively. Thus, the current ramp rate is conveyed as the Eq. 7.
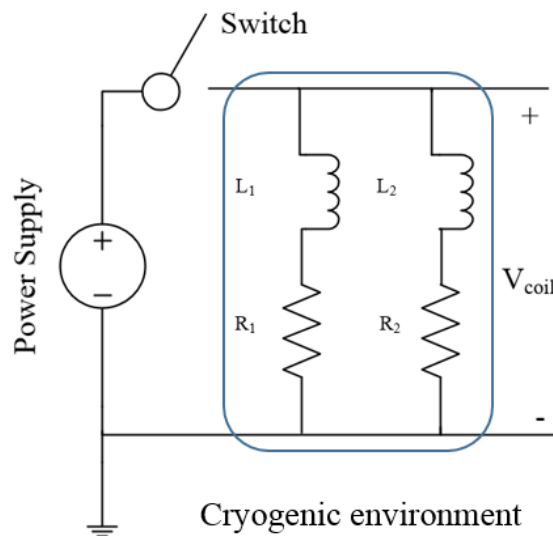
Fig. 13. A HTS coil equivalent circuit under fault condition

19

Where decay time τ is calculated by the relative between inductance and resistance of copper stabilizer as follows:

$$\tau = \frac{L_{cu}}{R_{cu}} = \frac{L_{cu}}{\rho_{cu} l_{cu}} A_{cu} \tag{8}$$

It is estimated that from the peak 116 A, current will drop to 0 A within 0.2 s where resistivity of copper $\rho_{cu} = 5.7 \times 10^{-10}$ (Ω.m) and inductance $L_{cu} = 0.185$ (μH) calculated by 3D FEA simulation. While ℓ_{cu} and A_{cu} are length and cross sectional area of copper stabilizer. Fig. 15 shows the average eddy current loss and eddy current density in cases of fault condition. It is remained 116 A steady state for 1 s, then suddenly discharged to 0 A within 0.2 s. In this case, the maximum eddy current is calculated 175 mW.

The motivation of this section analyzes the important losses of a current lead. They include eddy current loss of copper support parts be carried by 3D FEA simulation, and flux flow loss of HTS tapes calculated by applying numerical method. All these losses are conducted in terms of various current ramp rate at 10 A/s, 5 A/s and 2.5 A/s, and eddy current calculation, in cases of fault condition, is also proposed at the end. Moreover, the one of the detailed eddy current density distribution along the lead from 3D FEA simulation are shown in Fig. 14.

Fig. 14. Eddy current density simulation result of 10 A/s ramp rate at 2.9 second

(a)

(b)
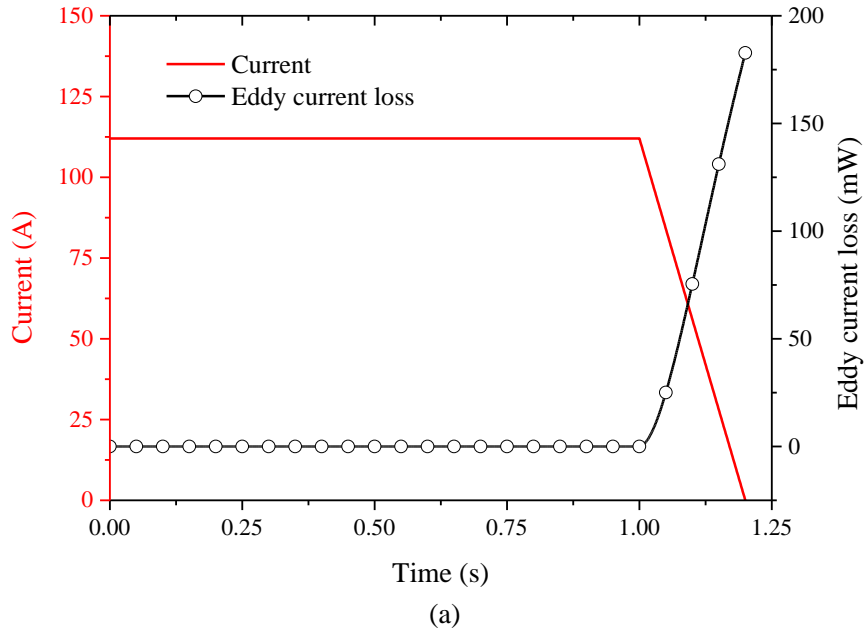
Fig. 15. Characteristic of (a) eddy current loss, (b) eddy current density of upper and lower copper support in cases of fault condition

2.2 Torque tube loss

Because the rotor houses superconducting coils, the temperature needs to be maintained around 30 K to keep the winding in the superconducting state with an acceptable critical current density. Therefore, most heat in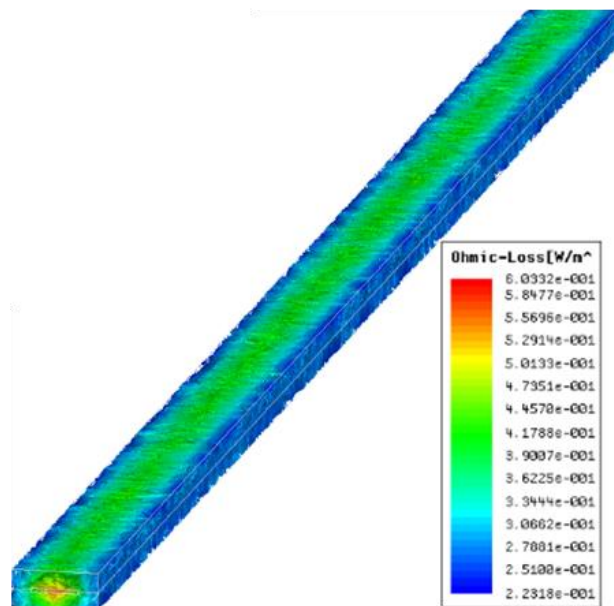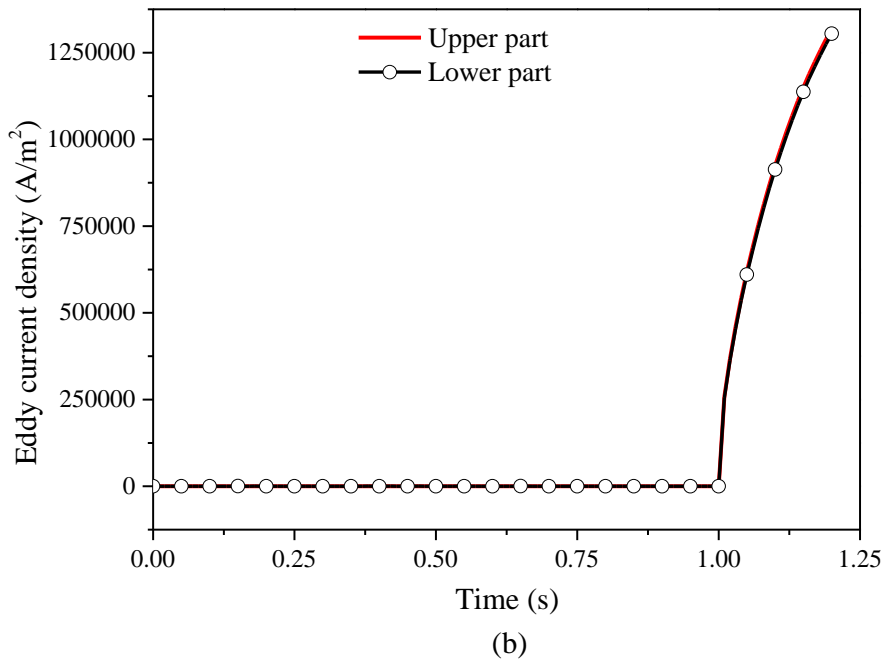vasion originates from heat conduction along the main rotor shaft with the two end at 300 K. G10 material is used to design the torque tubes because of its low thermal conductivity (k = 0.53 W/m.K). Considering the mechanical strength of G10 material, the designed transmission torque was 9554.14 kNm. Then, the torque tube conduction loss is calculated as follows:

$$Q_t = \frac{k_t A_t}{\delta_t} \Delta T \tag{9}$$

where Q_t is the conduction heat leak of the torque tubes, k_t is the thermal conductivity of the material which is dependent on temperature. ΔT, δ_t, A_t are the temperature difference, the length of the torque tubes and the equivalent cross-sectional area, respectively. Fig. 16 highlights the relative relationship of torque tube conduction loss on the inner diameter and torsion angle σ_t. For safety, the torsion angle σ_t must be within 0.2–0.3°. The optimal inner diameter was selected at 3.21 m because of less conduction heat loss and a safer conditions. The stress analysis and heat loss characteristics of the torque tubes is summarized in Table 10 for various length tubes.

Table 10. Stress analysis and heat loss of G-10 torque tube

	Case I	Case II	Case III	Case IV
Length [m]	0.40	0.60	0.80	1.0
Outer diameter D_{out} [mm]	3234	3234	3234	3234
Inner diameter D_{in} [mm]	3210	3210	3210	3210
Young's modulus [GPa]	18	18	18	18
Yield strength [MPa]	280	280	280	280
Poison ratio	0.19	0.19	0.19	0.19
Maximum shear stress [MPa]	49.03	49.03	49.03	49.03
Conduction heat loss [W]	86.90	57.94	43.45	34.76
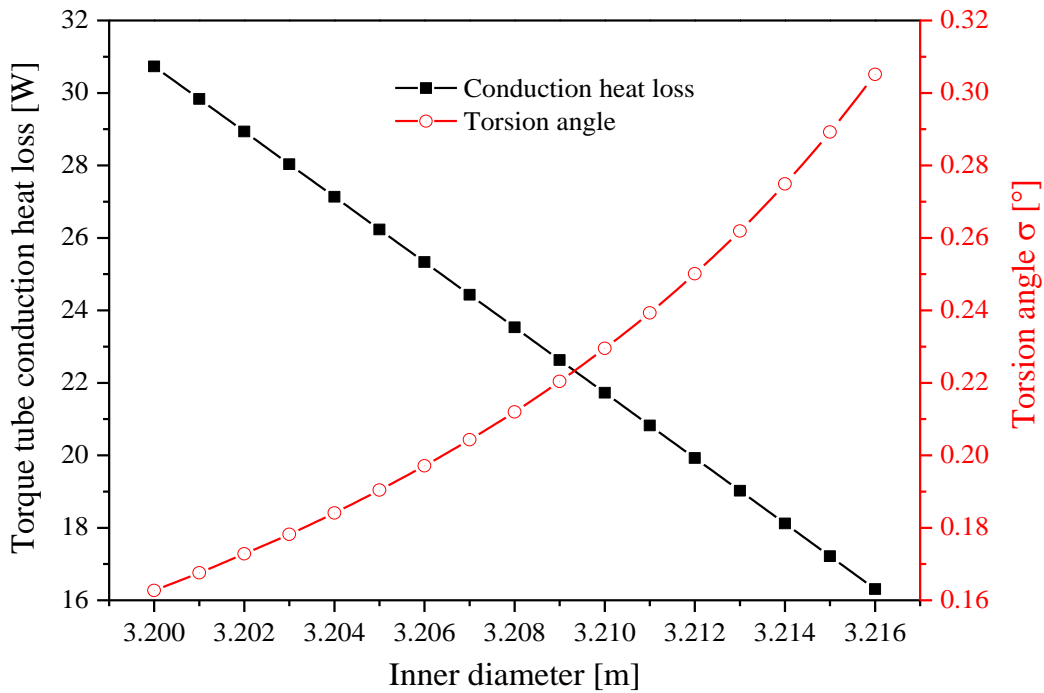
Fig. 16. Relative relationship between torque tube conduction loss, torsion angle and the inner diameter (at 0.8 m torque tube length)

HTS rotating machines require high torque and power to weight ratio. The weight and size of the machine need to be minimized during design. Superconductors can only operate at cryogenics temperatures in the 20-40 K range. The torque transfer components need to transmit mechanical torque between cryogenic and room temperature and, as a result, is exposed to high temperature gradient. Therefore, special care needs to be taken towards simulation of the temperature distribution, conducted heat and thermal stress distribution in the shaft.

Therefore, thermal strain of material is calculated as follow:

$$\Delta L = \alpha \Delta T L \tag{10}$$

where α is coefficient of thermal expansion (1/K), ΔT is temperature increase, L is initial length. Fig. 17 and Fig. 18 show the steady state temperature distribution of torque tube and local value of the displacement as well as the dimension change of the shaft, respectively. The 8 meter long shaft gets 21 mm shorter after cool-down.
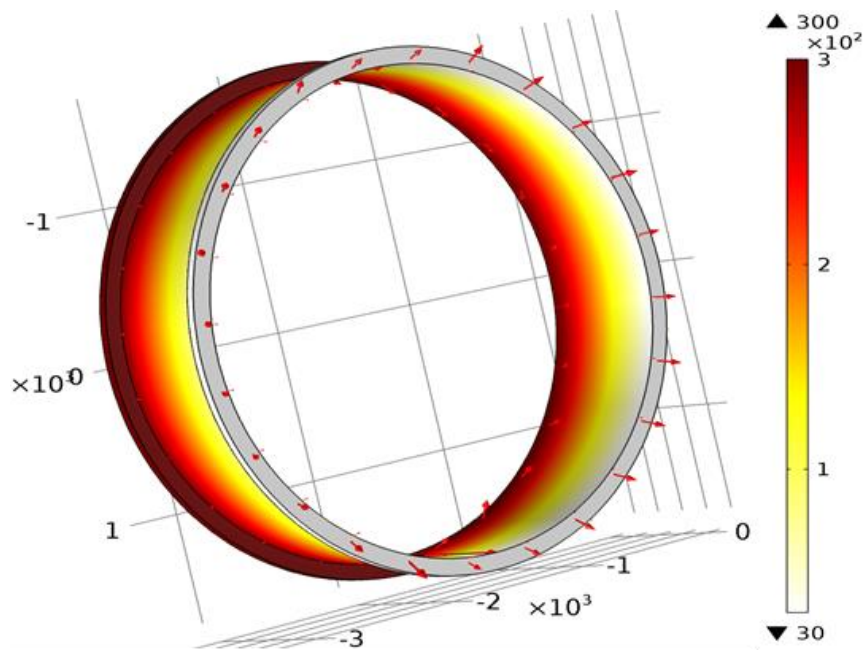
Fig. 17. Surface temperature distribution along the length of torque tube
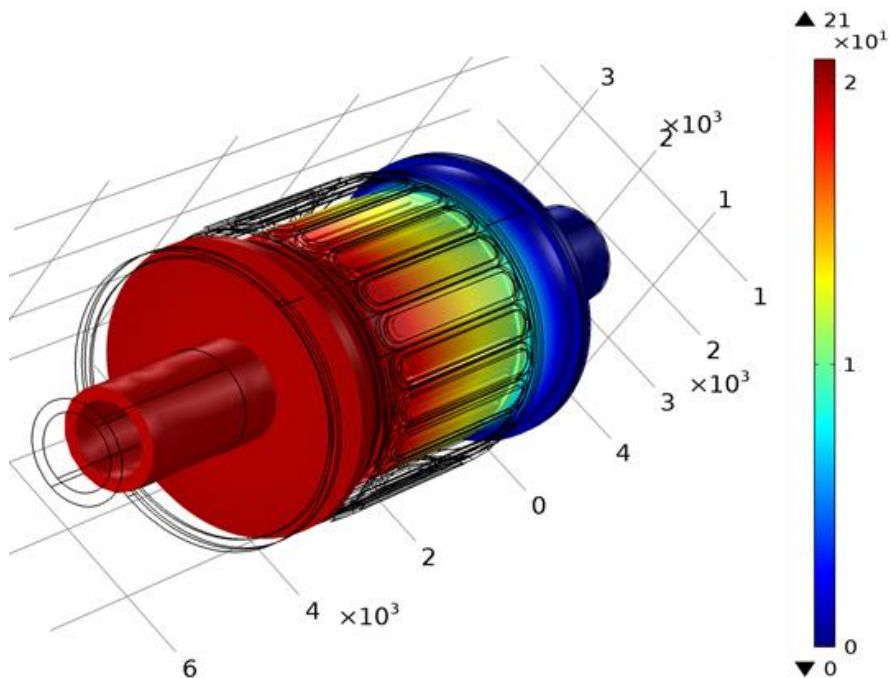
Fig. 18. Multiple torque tube characteristic (a) temperature distribution along the torque tube, (b) shaft deformation because of thermal strain

2.3 Radiation loss

A significant decrease in radiation heat loss can be achieved by wrapping the HTS coil with superinsulation layers. Radiation loss between the enclosure and the thermal shield with the presence of superinsulation layers number N_i is estimated as:

$$Q_r = \frac{\varepsilon\sigma}{N_i + 1}\left(T_w^4 - T_c^4\right) \tag{11}$$

where ε is the effective total thermal emissivity of the materials, and σ is Stefan-Boltzmann constant. T_w and T_c are the enclosure temperature and thermal shield temperature, respectively. As noted, the largest radiation heat flux $Q_r = 2.5$ W/m^2 (with 60 superinsulation layers) [17]. Then, radiation loss relies on radiation area S_r, which can be calculated by the rotor's dimensions.

Torque tube conduction loss is conversely proportional to torque tube length. In contrast, whenever torque tube length is increased, it will surely lead to radiation area S_r increases. As a result, radiation loss will linearly escalate. Subsequently, the optimal radiation loss is 106.45 W, where torque tube length is 0.8 m, as shown in Fig. 19.
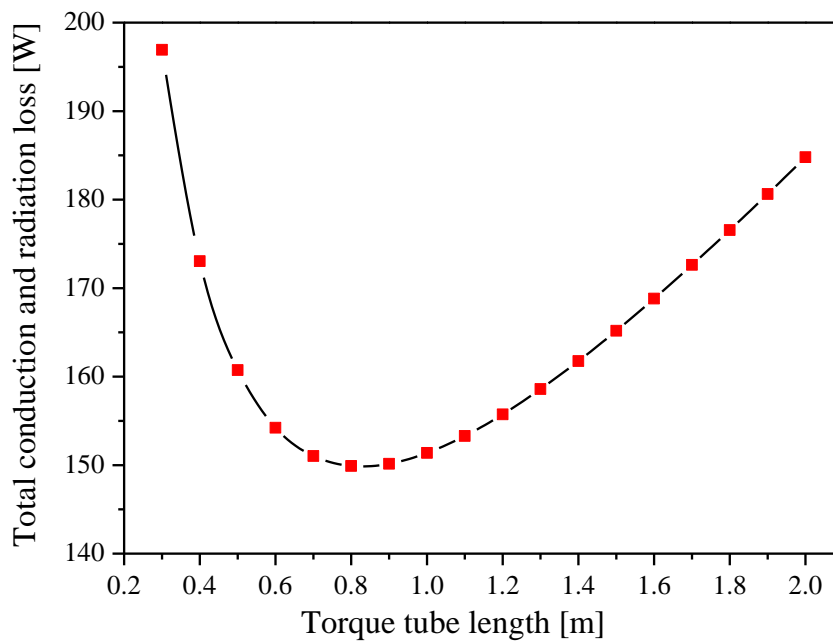
Fig. 19. Interdependence of torque tube length and radiation heat loss

2.4 Residual gas conduction loss

The residual gas, which mostly accounts for the outgassed surface of cryostat structural components, metals, and nonmetals, will be conducted, and the conduction heat loss of residual gas can be approximately given by [17]:

$$Q_g = \eta_g P_g S_g \Delta T \tag{12}$$

where the accommodation coefficient η_g depends on the warm temperature T_{wm} and the cold temperature T_{cl}. P_g is the pressure of the gas in the Dewar. ΔT, S_g are the different temperatures between the first thermal shield and the high temperature superconducting coils, and the cross-section facing the radiation shields, respectively.

2.5 Superconducting coils loss

2.5.1 Joule heating loss at mechanical lap joints

It is unavoidable to make joints in the tape length because of the limited availability of tape lengths from manufacturers. Total joint resistance is conveniently estimated as 0.05 μΩ. Consequently, Ohmic Joule heat loss can be calculated as follows [17].

$$Q_j = N_j I^2 R_j \tag{13}$$

where Q_j, I, R_j, N_j are the Joule heating loss, operating current, total joint resistance, and total number of mechanical lap joint of HTS tapes, respectively. The total HTS wire length is 1036 km at its highest efficiency 96.71%. Then, the N_j is 3453 joints where the routinely manufacturing long single-piece HTS length is 100–300 m. Therefore, Q_j is estimated 9.29 W.

2.5.2 Eddy current loss

Another loss that must be handled is the eddy current loss. The formula for its energy density in the low frequency limit for a tape (width: w; thickness: δ) is indicated as follows [17]:

$$e_{ed} = \frac{4\pi^2 \left(\mu_0 \lambda H_m\right)^2}{24\rho_m \tau_m} \tag{14}$$

where H_m and μ_0 are magnetic field and the permeability of free space (4π x 10^{-7} H/m). λ is the fraction of superconductor in the composite cross-section. While ρ_m and τ_m are the matrix resistivity and the natural time constant of the system, respectively.

2.5.3 Index loss

$$\frac{dI_{op}}{dt} = -\frac{E_c}{L_m I_c} \left(\frac{I_{op}}{I_c}\right)^n l_{mx} \tag{15}$$

Index loss depends on the intrinsic n-value HTS materials. It is necessary to consider the index voltage only in the maximum field region. By integrating the E_c electric field criterion over a conductor length l_{mx} we can see that the resistive voltage causes a current decay in the magnet of inductance L_m with operation current I_{op} and critical current I_c. That can be expressed as Eq. 15 [17]:

2.6 Supporting rods conduction loss and heat exchanger convection loss
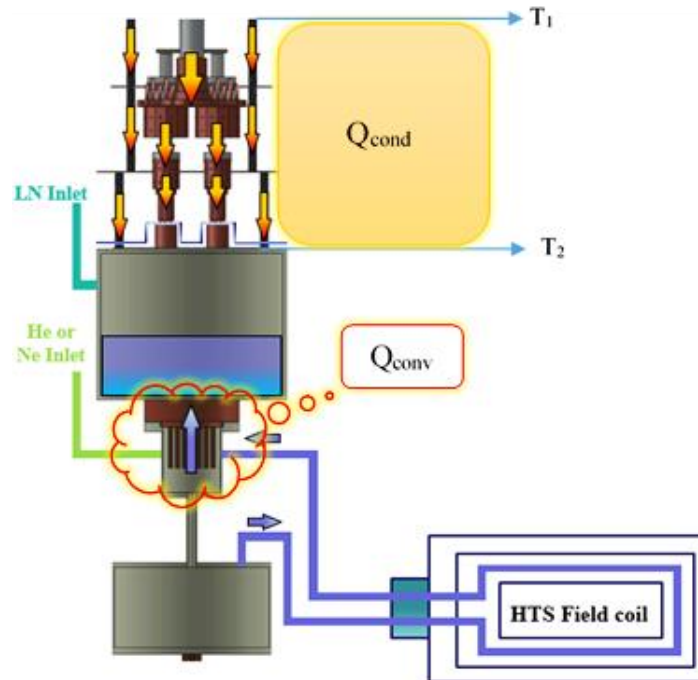
Fig. 20. Conduction of supporting rods and convection of heat exchanger

First, the thermal conduction by G10 rods between the enclosure and the thermal shield is estimated by Fourier's law as the conduction loss of torque tubes explained above. Fig. 20 shows the conduction of supporting rods, convection of heat exchanger.

Second, the thermal convection from the cold heat of heat exchanger as the natural convection cooling of finned surface. One would be expressed by the following [18]:

$$Q_{conv} = h_c A_c (T_s - T_b) \tag{16}$$

$$S_{opt} = 2.714 \frac{l_{fin}}{Ra^{1/4}} \tag{17}$$

$$h_c = 1.31 \frac{k_c}{S_{opt}} \tag{18}$$

where h_c is the individual heat transfer coefficient, A_c is the heat transfer surface area, T_s is the surface temperature and T_b is the bulk high temperature. In addition, the optimum fin spacing for a vertical heat sink is given by Rohsenow and Bar-Cohen for a given schematic in Fig. 21. Where ℓ_{fin} is the characteristic length in Ra number. All the fluid property are determined at the film temperature. The correlation of heat transfer coefficient h_c for the optimum spacing S_{opt} are generally given as Eq. 18:
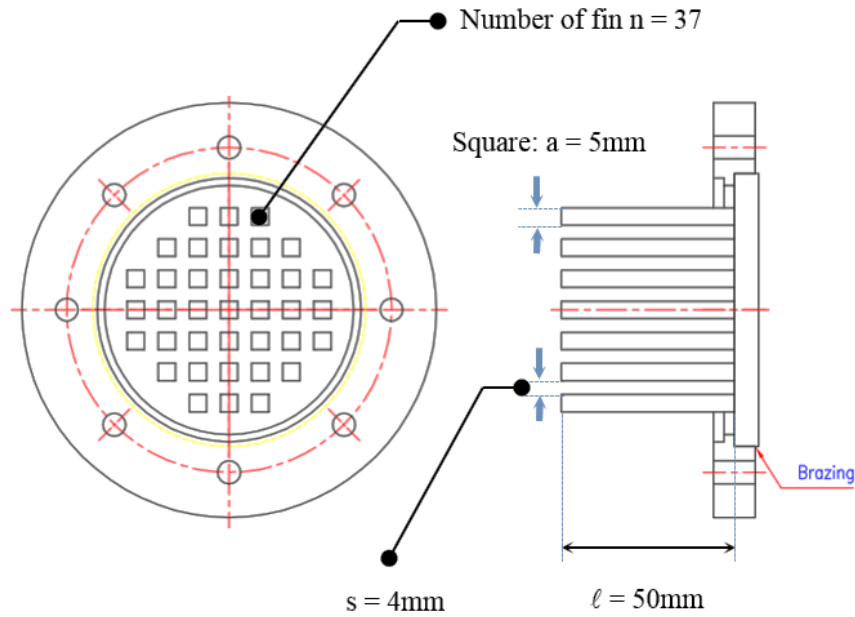
Fig. 21. Conceptual design of finned heat exchanger

Table 11. Total thermal loss estimation

Quantity	Value [W]
Lap joints Joule heating loss	9.29
Conduction via rods and convection via heat exchanger	9.33
Residual gas conduction	9.79
Eddy current loss and index loss	20.33
Current leads conduction loss	34.35
Torque tube conduction loss	43.45
Radiation loss	106.45
Total loss	233
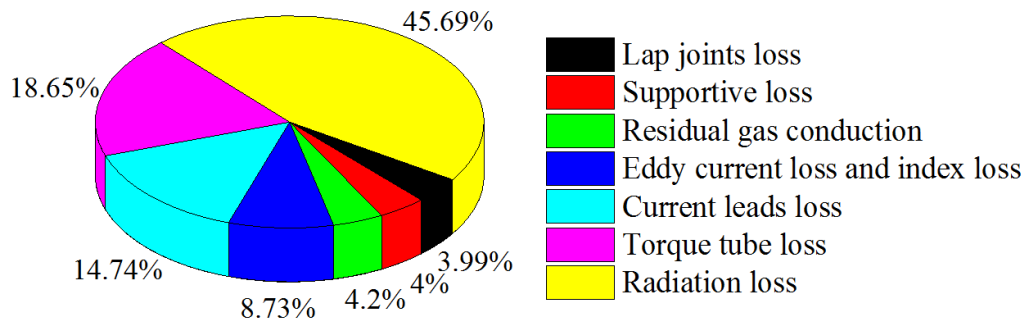
Fig. 22. Thermal loss ratio of a 10 MW-class HTS generator

A detailed summary of each heat loss of cooling system for the 10 MW-class HTS synchronous generator is listed in Table 11. Correspondingly, the total estimation heat loss, or Q_{total}, is 233 W. Although, by taking advantages of highly reflecting radiation shields separated by insulators in high vacuum, radiation is still the largest loss gain the top spot, 45% of total losses 106 W. There is no doubt that effectively applied numerical method to design torque tubes and current leads we can remarkably eliminate conduction losses. Hence, torque tubes conduction is reliably in the second spot 43 W, and current leads loss is a distant third 34 W. Where the three other losses – mechanical lap joints Joule heating loss, conduction loss of supporting rods and convection loss of heat exchangers, and residual gas conduction loss are almost the same rank around 9 W of each. It will surely now be apparent that calculating superconducting losses (eddy current loss and n-value intrinsic loss) can be a very complicated business, we give an equal estimation to 1% of total other losses over 20 W.

Chapter 3. Cryogenic Cooling System Design and Analysis

3.1 Cooling devices

Recently, many superconducting magnet systems have been required to use cryocoolers alone as the heat sink combination to liquid helium or nitrogen. Therefore, cryocooler performance and reliability are continuing improving. Consequently, there are more and more frequently implemented by physicists in their laboratory experiments or for commercial applications. The five kinds of cryocoolers most commonly used to provide cryogenic temperatures for various applications are the Joule-Thomson, Brayton, Stirling, Gifford-McMahon (G-M), and Pulse Tube (PT).

Cooling of superconducting electronics, magnets, and power systems is the main application of cryocoolers. However, it is useful to note that HTS power applications operating temperature range 30-40 K require considerably higher refrigeration powers at hundreds of watt. These applications include motors, and generations. For HTSSGs, the goal factors are the cryogenic system reliability, availability, capital cost and maintenance cost, as well.

Fortunately, the development of G-M cryocoolers line that would benefit the large scale of synchronous machines would include increases in unit performance from about 100 W at 30 K to several hundred watts and increases in reliability and required maintenance intervals. While development of PT cryocoolers are also under investigation for these applications because of their potential for higher efficiency and higher efficiency. However, right now G-M cryocoolers are widely used because of their advantages compared to PT cryocoolers listed in Table 12 [19].

Table 12. The different between PT cryocoolers and GM cryocoolers

Criteria	PT Cryocoolers	G-M Cryocoolers
Price	More expensive	Less expensive
Orientation	Only function properly in a purely vertical orientation	Can operate in any orientation

3.2 Configuration of cooling method

As stated above, evaporative cooling is applied in this thesis because it is a common way to cool HTS coils by submerging them in the liquid cryogens (liquid nitrogen or helium). This method is widely used in HTS turbo-generators and MRI machines for high security. As the dimensions of synchronous wind generator and the size of superconducting coils in this machine are both large, a large amount of cryogens would be needed to pre-cool the cryostat and cool the superconducting coil. Moreover, forced flow cooling with liquid cryogens is an effective method to exchange heat between cryogens and superconducting coils. Fig. 23 shows the configuration of the cooling system for a HTS synchronous generator. It is easily seen that, the liquid cryogen will flows into the superconducting coils by using circulating pump to liquid cryogen feed line. Then it returns by return line after it removing the heat rise in the field coil. The returned gas cryogen will be cooled again by the natural convection occurred in the heat exchanger [20].
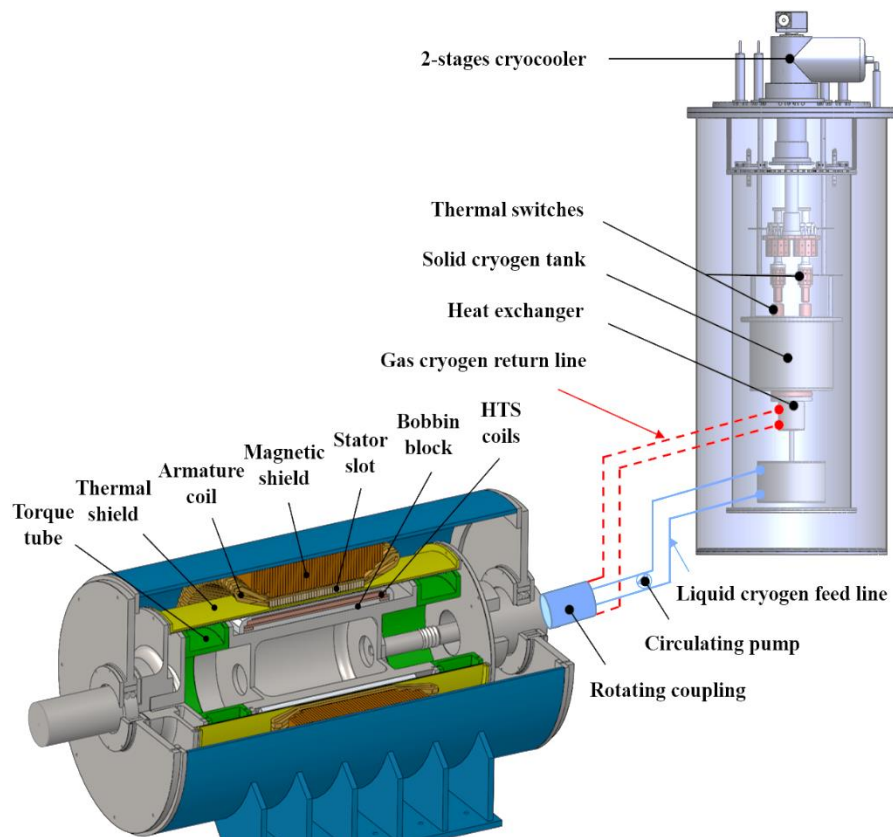

Fig. 23. Configuration of the cooling system for a HTS synchronous generator
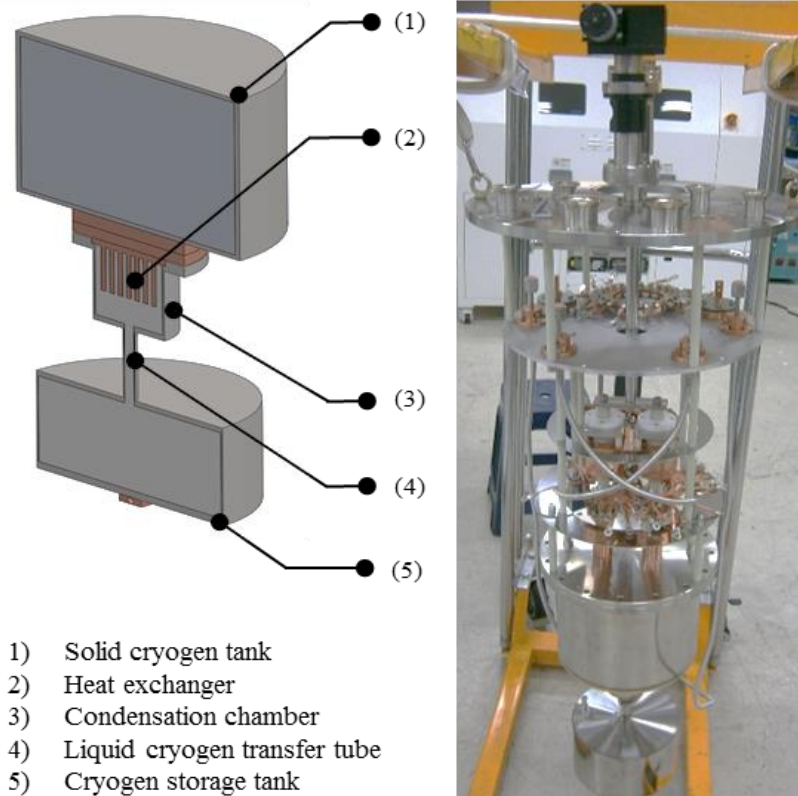
Fig. 24. Schematic of a 3D drawing model of solid cryogen cooling system via copper heat exchanger (left), and prototype of cooling device for superconducting rotating machines using a thermal trigger switch (right)

In addition, Fig. 24 presents the primary components that comprise the prototype of the cryogenic cooling system. The system can be classified into four main parts: a cold head, a thermal trigger switch, a cryogen tank and a heat exchanger with thermo-syphon technique. In addition, the detailed schematic of the solid cryogen tank, which is the main cooling source based on conduction method via copper heat exchanger, is also illustrated.

The device's principle application is to eliminate parasitic heat loss. As shown in Fig. 25, in case of normal operations, cryogen for cooling HTS field coils is made through the cryocooler. However, whenever the failure of the cryocooler occurs because of heat intrusion increases from room temperature, the cooling load is rapidly increased. In order to minimize the heat intrusion from room temperature, a trigger switch disconnects to the thermal trigger switch sockets.
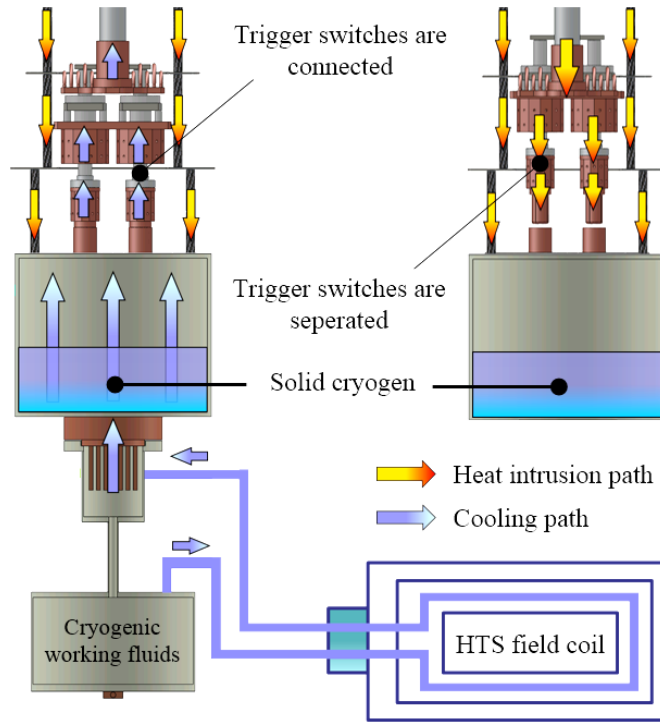
Fig. 25. The principle operation of a cooling system using thermal trigger switches at normal operation (left), and thermal trigger operating switches (right)

The duration for the system to remain detached from its cooling source is arbitrarily selected as 24 h. Then, to create an optimal design of a solid cryogen cooling system, it is essential to obtain the total volume of solid cryogen vessel. The total volume of the solid cryogen vessel V_{sc} is determined by the following equation:

$$V_{sc} = \frac{Q_{total}}{\Delta H} \Delta t \tag{19}$$

where Q_{total} is the total heat loss of the cooling system, and Δt is the duration of the temperature variation of solid cryogen from the initial temperature (T_i) to the final temperature (T_f). The total enthalpy change of solid cryogen ΔH is expressed as:

$$\Delta H = \int_{T_i}^{T_f} C_p(T) dT \tag{20}$$

where C_p is the specific heat of the solid cryogen, which is highly dependent on the temperature of the materials.

3.3 Solid cryogens

The field coil is capable of increased performance, in a given magnetic field, as we lower the operating temperature. To achieve a useful field from our magnet, we needed to cool the field coil to at least 77 K, and keep at or below this temperature for a period of approximated 24 hours. This left us with two options – either we base our design on cryogens with a boiling point below 77 K, or we could freeze a cryogen to the required temperature.

Then a number of factors were carefully considered when selecting nitrogen as the optimum cryogen to use for this cryogenic system. First, the cost is less expensive in comparison to other cryogens because of its availability. Second, it has a higher specific heat capacity (per unit mass) than other common cryogens such as neon and argon. Third, incases of hydrogen, it has the disadvantage of being potentially hazardous of explosion, and it would have been difficult to ensure its safe deployment within this scale of this large scale power rating. Moreover, the latent heat of solid nitrogen goes through a solid-solid phase transition at 35.6 K, increasing solid cryogen's ability to absorb heat although liquid nitrogen freezes at 63.2 K as illustrated Fig. 26. Thus, it can initially be cooled below this point.

It was decided therefore that the thermal battery should be cooled to 20 K using frozen nitrogen, and the magnet should be operated between $T_i = 20$ K and $T_f = 63.16$ K (below the freezing point of nitrogen). Having set these parameters, we then went on to investigate the suitability of solid nitrogen as a means for absorbing heat over this temperature range. Within a 24 h duration and a total heat loss (Q_{total}) of 233 W, the volume of solid nitrogen as a solid cryogen (285 L) is about 65% less than solid argon (469 L) and over four times smaller than solid neon (1,176 L), as shown in Fig. 27. Moreover, Fig. 27 also illustrates the total volume of solid cryogens according to different temperature ranges. A wider range of temperature will lead to smaller amount of cryogen volume used. Solid nitrogen from 63.16 K to 20 K is much more effective than the 4 K level because the difference total volume is insignificant, just 21 L, while the cooling process cost and difficulty requires much effort.
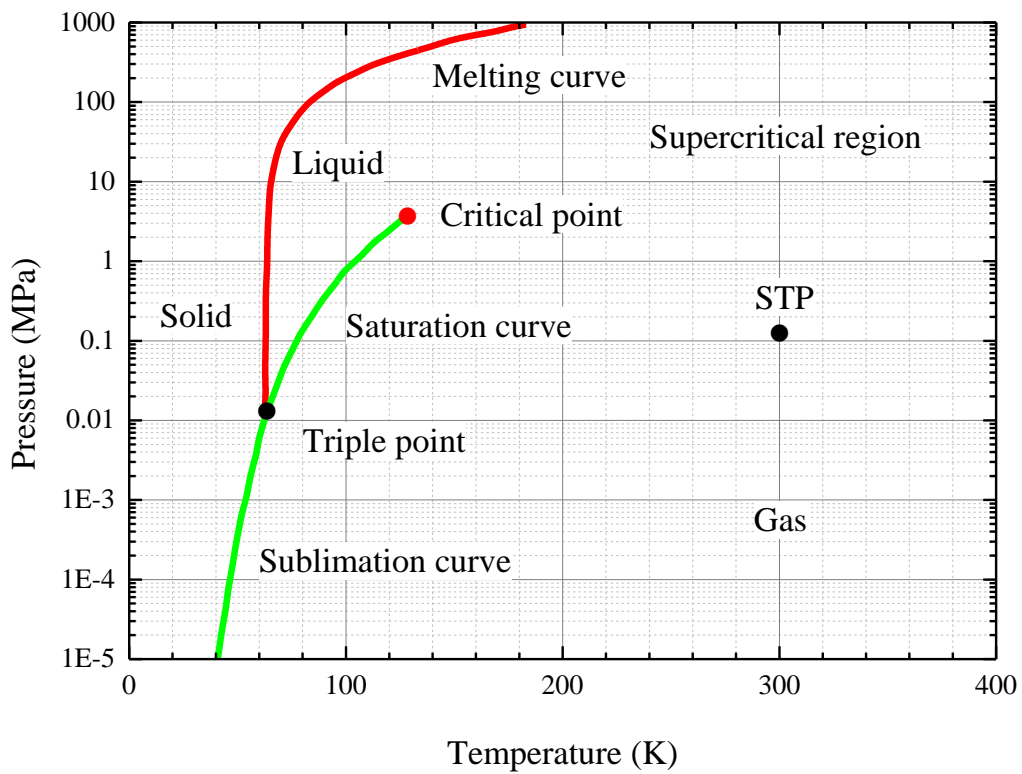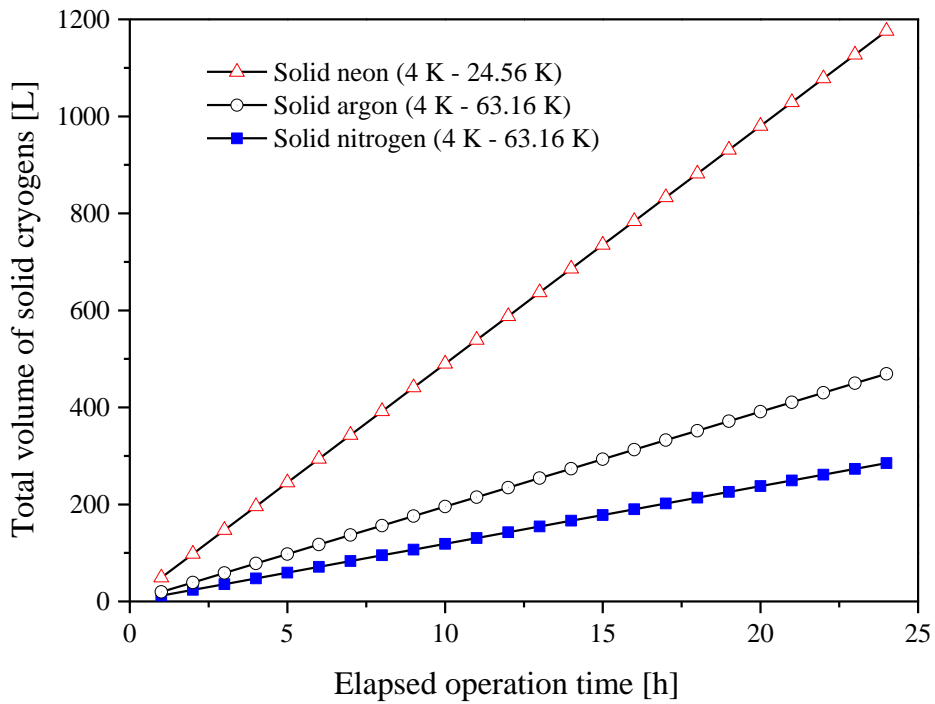
(a)
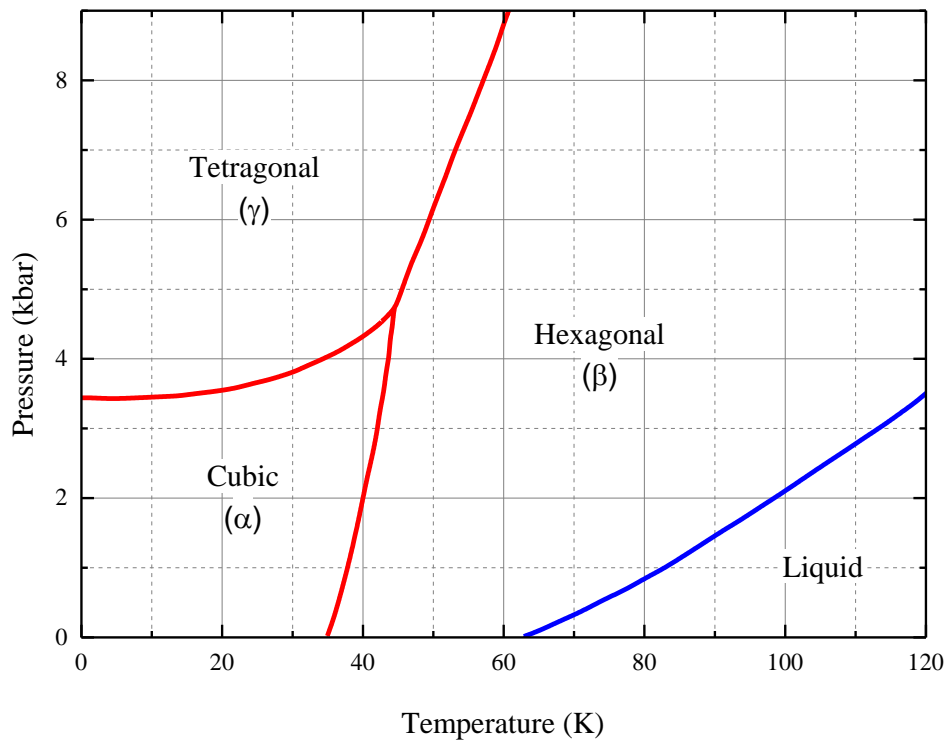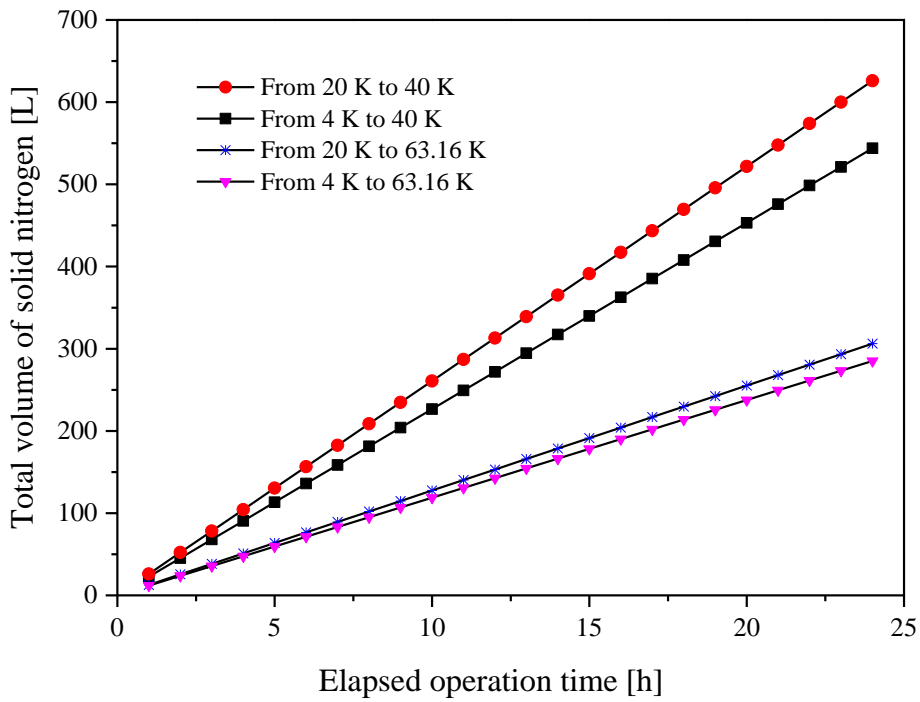

(b)

Fig. 26. Phase diagram of nitrogen (a) three phases diagram and (b) α-β-γ solid phase transition

(a)

(b)

Fig. 27. The various calculated values of (a) total volume different solid cryogens versus Δt (b) the total volume of solid nitrogen varying on Δt and different initial temperature and the final temperature range

Chapter 4. Conclusion

First, it underlines the following considerations for improved electrical connections to rotating superconducting winding (current leads). The total refrigerator power demanded by the current lead is minimized for an infinite set of mass flow current combinations. Along this line, the lead axial temperature distribution remains unchanged. The self-sufficient operating line approximates closely the line of thermodynamically optimum operating conditions.

Second, to establish the following design considerations for improved superconducting mechanical connection (torque tubes). A major reduction in the torque tube refrigerator power can be realized by intercepting most of the conduction heat leak at an intermediate temperature.

Finally, a high performance, reliability, and optimal cooling system has been characterized in this study. The device's principle application is to eliminate parasitic heat loss from systems' non-operating cryocoolers. Therefore, it can utilize cryocooler redundancy and downplay the cryogen usage in Dewar systems. Because of the significant savings in refrigeration power, cryogen consumption can be achieved with a short investment return time period and at a relatively low cost. In cases of cryocooler failures, it is estimated that 306 L (306 L* $0.91/L ~ $278) (University Research Instrumentation Center price list, 2014) of solid nitrogen is used to keep the cryostat, whose total optimum heat leak is 233 W, constantly operated within a 24 h period between 20 K and 63.16 K.

This thesis concludes that improvements are possible in the design of a cryogenic cooling system for a rotating superconducting winding. It suggests that the future development work can incorporate the conclusions offered here into the complete system design of a large superconducting rotor. Another possible more immediate objective is the investigation of the transient state behavior and thermal performance of this class of complex cryogenic system. In future, the optimization work on newer systems should pay more attention to the mechanical design and its interdependence with the overall thermal performance of the cryogenic system.

Declaration

I herewith declare that this thesis was composed by myself under the supervision of Professor Ho Min Kim at Electrical Engineering Department, College of Engineering, Jeju National University from Sep 2013 to May 2015 without the prohibited assistance of third parties and without making use of aids other than those specified, and that this work has not been submitted for any other degree of professional qualification except as specified. Significant parts of the work outlined in this thesis have been published:

◆ Chapter 1 is based on: "Status of the technology development of large scale HTS generators for wind power turbine", T. D. Le, et al, *Progress in Superconductivity and Cryogenics* (Accepted on June 2015).

◆ Chapter 2 is based on the two following articles. Moreover, the work in Chapter 2 provided the basis and led directly to the *International Conference on Coated Conductors for Applications 2014*, Jeju-si, S. Korea.

"Conceptual design of current lead for large scale high temperature superconducting rotating machine", T. D. Le, et al, *Progress in Superconductivity and Cryogenics*, vol 16 (2), pp. 54-58, 2014.

"Transient characteristics of current lead losses for the large scale high-temperature superconducting rotating machine", T. D. Le, et al, *Progress in Superconductivity and Cryogenics*, vol 16 (4), pp. 62-65, 2014.

◆ Chapter 3 is based on the two following articles. Furthermore, the work in Chapter 3 also provided the basis and led directly to the *Applied Superconductivity Conference 2014*, Charlotte, N.C, United States and the *International Joint Conference on Convergence 2015*, Ho Chi Minh, Vietnam, respectively.

"Thermal design of a cryogenics cooling system for a 10 MW-class high-temperature superconducting rotating machine", T. D. Le, et al, *IEEE Transactions on Applied Superconductivity*, vol 25 (3), p. 3800305, 2015.

"Thermal analysis of a cooling system for a high-temperature superconducting magnet system", T. D. Le, et al, *The Journal of the Institute of Internet, Broadcasting and Communication* (Accepted on June 2015).

Jeju-si, June 2015

Le Thanh Dung

List of Publications

[1] J. H. Kim, S. I. Park, **T. D. Le**, K. L. Kim, H. G. Lee, Y. S. Jo, Y. S. Yoon, H. M. Kim, "Characteristic Analysis of Various Structural Shapes of Superconducting Field Coils", *IEEE Transactions on Applied Superconductivity*, vol. 25 (3), p. 5201105, 2015.

[2] **T. D. Le**, J. H. Kim, S. I. Park, D. H. Kang, H. G. Lee, Y. S. Jo, Y. S. Yoon, H. M. Kim, "Thermal Design of a Cryogenics Cooling System for a 10 MW-Class High-Temperature Superconducting Rotating Machine", *IEEE Transactions on Applied Superconductivity*, vol. 25 (3), p. 3800305, 2015.

[3] **T. D. Le**, J. H. Kim, S. I. Park, D. J. Kim, H. G. Lee, Y. S. Yoon, Y. S. Jo, K. Y. Yoon, H. M. Kim, "Transient characteristics of current lead losses for the large scale high-temperature superconducting rotating machine", *Progress in Superconductivity and Cryogenics*, vol. 16 (4), pp. 62-65, 2014.

[4] S. I. Park, J. H. Kim, **T. D. Le**, D. H. Lee, D. J. Kim, Y. S. Yoon, K. Y. Yoon, H. M. Kim, "Analysis of losses within SMES system for compensating output fluctuation of wind power farm", *Progress in Superconductivity and Cryogenics*, vol. 16 (4), pp. 57-61, 2014.

[5] J. H. Kim, S. I. Park, **T. D. Le**, H. C. Jo, Y. S. Jo, Y. H. Choi, H. G. Lee, H. M. Kim, "Analysis of the Mechanical Characteristics of a 17-MW-Class High-Temperature Superconducting Synchronous Motor", *Journal of Superconductivity and Novel Magnetism*, vol. 27 (9), 2014.

[6] J. H. Kim, S. I. Park, **T. D. Le**, H. M. Kim, "3D electromagnetic design and electrical characteristics analysis of a 10-MW-class high-temperature superconducting synchronous generator for wind power", *Progress in Superconductivity and Cryogenics*, vol. 16 (2), pp. 47-53, 2014.

[7] **T. D. Le**, J. H. Kim, S. I. Park, H. M. Kim, "Conceptual design of current lead for large scale high temperature superconducting rotating machine", *Progress in Superconductivity and Cryogenics*, vol. 16 (2), pp. 54-58, 2014.

[8] S. I. Park, J. H. Kim, **T. D. Le**, H. M. Kim, "Comparison of superconducting generator with 2G HTS and MgB2 wires", Progress in Superconductivity and Cryogenics, vol. 15 (4), pp. 48-52, 2013.

References

[1]   *World Energy Investment Outlook*, International Energy Agency, 2014.

[2]   *New record in worldwide wind installations*, World Wind Energy Association, 2015.

[3]   J. Lloberas, A. Sumper, M. Sanmarti, X. Granados, "**A review of high temperature superconductors for offshore wind power synchronous generators**," *Renewable and Sustainable Energy Reviews*, vol. 38, pp. 404-414, 2014,

[4]   W. Tong, *Wind Power Generation and Wind Turbine Design*. Southampton, WIT Press, 2010.

[5]   G. Snitchler, B. Gamble, C. King, and P. Winn, "**10 MW class superconductor wind turbine generators**," *IEEE Trans. Appl. Supercond.,* vol. 21, no. 3, pp. 1089–1092, 2011.

[6]   N. Goudarzi and W. D. Zhu, "**A review on the development of wind turbine generators across the world**," *Int. J. Dynam. Control*, vol. 1, no. 2, pp. 192-202, 2013.

[7]   V. Matias, and R. H. Hammond, "**HTS superconductor wire: $5/kAm by 2030**," *CCA2014 Conference*, S. Korea, ID: LL_IS_002, 2014.

[8]   S. H. Moon, "**Recent progress of 2G superconducting wire in SuNAM**," *CCA2014 Conference*, S. Korea, ID: LL_IS_003, 2014.

[9]   B. Chen, G. B. Gu, G. Q. Zhang, F. C. Song, and C. H. Zhao, "**Analysis and design of cooling system in high temperature superconducting synchronous machines**," *IEEE Trans. Appl. Supercond.*, vol. 17, no. 2, p. 1557, 2007.

[10]   J. A. Urbahn, R. A. Ackermann, X. Huang, E. T. Laskaris, K. Sivasubramaniam, and A. Steinbach, "**The thermal performance of a 1.5 MVA HTS generator**," *AIP Conference Proceedings 710*, p. 849, 2004.

[11]   G. Snitchler, B. Gamble, and S. S. Kalsi, "**The performance of a 5 MW high temperature superconductor ship propulsion motor**," *IEEE Trans. Appl. Supercond.*, vol. 15, no. 2, pp. 2206-2209, 2005.

[12] B. Haid, H. G. Lee, Y. Iwasa, S. S. Oh, H. S. Ha, Y. K. Kwon, and K. S. Ryu, "**Stand-alone solid nitrogen cooled 'permanent' high-temperature superconducting magnet system**," *IEEE Trans. Appl. Supercond.*, vol. 11, no. 1, pp. 2244-2247, 2001.

[13] J. H. Kim and H. M. Kim, "**Electromagnetic design of 10 MW-class superconducting wind turbine using 2G HTS wire**," *Progress in Superconductivity and Cryogenics*, vol. 15, no. 3, pp. 29–34, 2013.

[14] J. H. Kim, S. I. Park, T. D. Le, and H. M. Kim, "**3D electromagnetic design and electrical characteristic analysis of a 10-MW-class high temperature superconducting synchronous generator for wind power**," *Progress in Superconductivity and Cryogenics*, vol. 16, no. 2, pp. 47–53, 2014.

[15] T. D. Le, J. H. Kim, S. I. Park, and H. M. Kim, "**Conceptual design of current lead for large scale high temperature superconducting rotating machine**," *Progress in Superconductivity and Cryogenics*, vol. 16, no. 2, pp. 54–58, 2014.

[16] T. D. Le, J. H. Kim, S. I. Park, D. J. Kim, H. G. Lee, Y. S. Yoon, Y. S. Jo, K. Y. Yoon, and H. M. Kim, "**Transient characteristics of current lead losses for the large scale high-temperature superconducting rotating machine**," *Progress in Superconductivity and Cryogenics*, vol. 16, no. 4, pp. 62–65, 2014.

[17] Y. Iwasa, *Case Studies in Superconducting Magnets: Design and Operational Issues*, New York, Springer 2nd ed., 2009.

[18] M. Thirumaleshwar, *Fundamentals of Heat and Mass Transfer,* Pearson Education 2nd ed., 2009.

[19] R. Radebaugh, "**Cryocoolers: the state of the art and recent developments**," *J. Phys.: Condens, Matter*, vol. 21, p. 164219, 2009.

[20] T. D. Le, J. H. Kim, S. I. Park, D. H. Kang, H. G. Lee, Y. S. So, Y. S. Yoon, and H. M. Kim, "**Thermal design of a cryogenics cooling systems for a 10 MW-class high-temperature superconducting rotating machine,**" *IEEE Trans. Appl. Supercond.*, vol. 25, no. 3, p. 3800305, 2015.